Poly(allylamine)-tripolyphosphate polymeric nanoparticle as an NLRP3-dependent systemic adjuvant for the vaccine development

Gastón P. Rizzo[1], Rodrigo C. Sanches[2], Camila Chavero[1], Daiana S. Bianchi[1], Eugenia Apuzzo[3], Santiago E. Herrera[4], Maximiliano L. Agazzi[5], Irene A. Keitelman[6], Analía S. Trevani[6], Sergio C. Oliveira[2, 7], Omar Azzaroni[3], Paola L. Smaldini[1 †], Guillermo H. Docena[1 †].*

[1]Instituto de Estudios Inmunológicos y Fisiopatológicos (IIFP), UNLP, CONICET, asociado a CIC PBA, Facultad de Ciencias Exactas, Departamento de Ciencias Biológicas, La Plata, Argentina (IIFP-UNLP-CONICET).

[2]Department of Biochemistry and Immunology, Institute of Biological Sciences, Federal University of Minas Gerais (ICB-UFMG).

[3]Instituto de Investigaciones Fisicoquímicas Teóricas y Aplicadas (INIFTA), (UNLP, CONICET), 1900 La Plata, Buenos Aires, Argentina.

[4]Instituto de Química de los Materiales, Ambiente y Energía (INQUIMAE), UBA, CONICET, Facultad de Ciencias Exactas y Naturales, Departamento de Química Inorgánica Analítica y Química Física. Buenos Aires, Argentina.

[5]Instituto para el Desarrollo Agroindustrial y de la Salud (IDAS), (UNRC, CONICET), Ruta Nacional 36 KM 601, 5800 Río Cuarto, Argentina.

[6]Laboratorio de Inmunidad Innata, Instituto de Medicina Experimental (IMEX), CONICET, Academia Nacional de Medicina, Buenos Aires, Argentina.

[7]Department of Immunology, Institute of Biomedical Sciences, University of São Paulo, São Paulo, Brazil

[†]Shared senior authorship

***Corresponding author:** Paola L. Smaldini; psmaldini@biol.unlp.edu.ar

ABSTRACT

Nanotechnology plays a crucial role in vaccine development and provides the opportunity to design functional nanoparticles (Np) of different compositions, sizes, charges and surface properties for biomedical applications. The present study aims to evaluate a complex coacervate-like Np composed of poly(allylamine hydrochloride) (PAH) and tripolyphosphate (Tpp) as a safe vehicle and adjuvant for systemic vaccines. We investigated the activation of different antigen-presenting cells (APCs) with Np-PAH and its adjuvanticity in Balbc/c and different KO mice that were intraperitoneally immunized with Np-OVA.

We found that Np-PAH increased the expression of CD86 and MHCII and promoted the production and secretion of interleukin-1β (IL-1β) and IL-18 through the inflammasome NLRP3 when macrophages and dendritic cells were co-incubated with LPS and Np-PAH. We evidenced an unconventional IL-1β release through the autophagosome pathway. The inhibition of autophagy with 3-methyladenine reduced the LPS/Np-PAH-induced IL-1β secretion. Additionally, our findings showed that the systemic administration of mice with Np-OVA triggered a significant induction of serum OVA-specific IgG and IgG2a, an increased secretion of IFN-γ by spleen cells, and high frequencies of LT $CD4^{+}IFN\text{-}\gamma^{+}$ and LT $CD8^{+}IFN\text{-}\gamma^{+}$. In conclusion, our findings show that PAH-based Np promoted the inflammasome activation of innate cells with Th1-dependent adjuvant properties, making them valuable for formulating of novel preventive or therapeutic vaccines for infectious and non-infectious diseases.

Keywords: Nanoparticle, Polymeric Poly(allylamine) nanoparticles, Adjuvant, Inflammasome, NLRP3, Systemic vaccines.

INTRODUCTION

Vaccines have prevented millions of deaths in the last decades (mainly in the pediatric population), reduced medical care costs, and allowed us to coexist peacefully with pathogens. The use of adjuvants in vaccines promoted enhanced protection by the induction of robust and perdurable immunity. In this sense, nanotechnology has significantly impacted vaccine development, as nanoparticles are associated with inherent physical properties to protect the antigen cargo and increase immunogenicity and protection[1–3]. Very recently, nanovaccines showed to be safe and effective for immune intervention in COVID-19[4–6].

One of the critical elements in nanoparticle technology for vaccine formulation is polymers. Among these, amine-based polymers are interesting macromolecules since they can act as polycations depending on the pH. Due to this property, polyamine can serve as a building block for the construction of nanoparticles that are stabilized exclusively by soft interactions like electrostatics. An example is the formation of nano-sized complex coacervates by the interaction between polyamines and multivalent salts like citrate, phosphates and polyphosphates[7,8]. Poly(allylamine) hydrochloride (PAH) is one of the most frequently explored polyamines since its composition can be accurately determined and possesses only one type of amine: primary amines. PAH also finds application in oral drug formulations, as ligands for anion exchange chromatography to facilitate the subsequent processing of bio-pharmaceutical products, as reagents in diagnostics, and in formulations of bactericides for use as antibiotics and antiseptics[9–12]. A common complexing agent for developing polyamine-based nanoparticles and soft complexes is phosphate[13,14]. In particular, the tripolyphosphate (Tpp) anion has multiple industrial applications (e.g., food

additive), is readily available, carries enough charge to act as an ionic crosslinker (up to 5 negative charges per ion), and is an FDA- and GRAS-approved chemical. By this, Tpp is one of the most used crosslinkers for synthesizing soft nanoparticles with biomedical applications[15]. As we recently demonstrated, the mixture of PAH and Tpp in an aqueous solution gives rise to the formation of a highly stable colloidal dispersion of complex coacervates, characterized by size and surface charge that enable the loading of proteins with different molecular weights and charges[16].

Organic and inorganic nanoparticles, including uric acid crystals, cholesterol crystals, silica crystals, calcium pyrophosphate crystals (pseudogout), asbestos, and aluminum salts, are capable of triggering innate immunity through the activation of the multiprotein complex known as the inflammasome in antigen-presenting cells (APCs)[17,18]. Recently, polyamine-based platforms, including polyethyleneimine, chitosan, and polylysine, have demonstrated attractive properties as adjuvants[19–21].

The innate immune response is initiated by recognizing specific conserved molecular patterns derived from microorganisms (MAMPs and PAMPs) and signals from host tissue damage (DAMPs). A new designation for molecular patterns has been coined for non-pathogenic nanoparticles as nanoparticle-associated molecular patterns or NAMPs[17,22]. PAMPs, DAMPs, and NAMPs interact with surface or intracellular pattern recognition receptors, initiating pro-inflammatory programs that activate innate cells[23,24]. In particular, NLRs detect NAMPs, and NLRP3 is the most extensively characterized cellular receptor[25]. It is primarily expressed in myeloid lineage cells, such as granulocytes, monocytes, macrophages, and dendritic cells. Nanoparticles promote lysosomal membrane permeabilization (LMP), and cathepsins are released into the cytosol[26]. Cathepsins are

cysteine proteases primarily found in late endosomes and lysosomes and play crucial roles in various physiological processes, maintaining their proteolytic activity at physiologic pH. These enzymes, mainly cathepsin B, can activate the NLRP3 inflammasome[27]. After the inflammasome activation, the adaptor protein ASC (apoptosis-associated speck-like protein containing a CARD) assembles into large helical fibers interacting with each other and forming aggregates. The recruitment of pro-caspase-1 to ASC promotes the autocatalytic activation of caspase-1, which leads to activating the pro-forms of IL-1β and IL-18 and the pore-forming cytosolic protein gasdermin-D (GSDMD). Upon cleavage of the N-terminal domain of GSDMD, these fragments oligomerize into a ring shape and insert into the plasma membrane, forming a pore through which IL-1β and IL-18 are released. Moreover, GSDMD permeabilizes the cell membrane, leading to ionic imbalance and subsequent osmotic lysis, triggering a form of inflammatory programmed-cell death known as pyroptosis, which can be observed by the release of the enzyme lactate dehydrogenase (LDH) into the extracellular environment[28,29]. However, cytokines can be secreted through an unconventional GSDMD–independent pathway, including intracellular vesicular trafficking (exocytosis of lysosomes or autophagosomes) or microvesicle release without inducing cell death[30,31]. For instance, multivesicular bodies (MVBs), loaded with endosomes containing the cytokine, undergo lysis upon release into the extracellular environment, releasing the soluble cytokine[32,33]. Moreover, there are non-canonical pathways of inflammasome activation that proceed through the proteolytic action of caspase-11[34,35].

The possibility that an immunogen encapsulated in PAH-based Np could trigger the immune system by activating innate cells, endowing them with migratory capacities

towards the lymph node to promote the activation of naive B and T cells, makes them potential candidates for vaccine formulation. The production of cytokines and chemokines, along with the expression of CD80, CD86, and MHCII on the cell surface, transforms these cells into APCs with an increased ability to activate T lymphocytes[36–38]. We previously found that the positive PAH-based nanoparticles are non-toxic and are internalized by phagocytic cells with intracellular localization in early and late endosomes[16]. In this study, we found that dendritic cells and macrophages undergo activation upon nanoparticle uptake, cell migration, and promotion of Th1-dependent adaptive immunity. The release of IL-1β and IL-18 through the NLRP3 activation triggered the secretion of IFN-γ with the induction of specific IgG antibodies.

MATERIALS AND METHODS

Preparation of PAH/Tpp nanoparticle

PAH/Tpp nanoparticles were prepared by following the procedure described in Apuzzo et al[16]. Briefly, $0.125\ V_f$ ml of PAH (17.5 kDa, Sigma-Aldrich, St. Louis, MO, USA) 40mM (monomer concentration) at pH 8.5, $0.75\ V_f$ ml of deionized water, and $0.125\ V_f$ ml of Tpp (Sigma-Aldrich, St. Louis, MO, USA) 24mM at pH 8.5 were mixed under constant stirring at room temperature (RT). The addition of Tpp was made very quickly in order to prevent the system from collapsing into a macroscopic phase. After this procedure, a volume V_f of dispersed PAH/Tpp nanoparticles is obtained with a final concentration of PAH and Tpp of 5mM and 3mM, respectively. In this work, the Np concentration was expressed in terms of PAH monomer concentration (i.e., 0.5mM Np means a 1:10 dilution of the original dispersion). The protein-loaded nanoparticle dispersions were prepared by following the same procedure but adding an aqueous solution of chicken egg albumin (OVA) (EndoFit(TM) InvivoGen, San Diego, CA, USA) at the water addition stage. The volume of deionized water was re-calculated as $V_{water} = 0.75\ V_f - V_{OVA}$ and the OVA volume was fixed to obtain the desired OVA concentration in the final solution.

The percentage of encapsulated OVA was calculated by assessing the protein content of the supernatant using bicinchoninic acid (BCA) commercial kit (Thermo Fisher Scientific, Waltham, MA, USA).

Cell lines

HEK-hTLR4-reporter (InvivoGen®, San Diego, CA, USA), HT-29 and J774 cell lines were maintained in DMEM medium (Gibco® Thermo Fisher Scientific, Waltham, MA,

USA) containing 10% FBS (Internegocios, Mercedes, Bs As, Argentina), 100U/mL penicillin and 100µg/mL streptomycin (Gibco® Thermo Fisher Scientific, Waltham, MA, USA). The THP1-ASC-GFP cell line was maintained in RPMI medium (Gibco® Thermo Fisher Scientific, Waltham, MA, USA) containing 10% FBS, 100U/mL penicillin and 100µg/mL streptomycin.

Bone marrow-derived macrophages (BMDMs) were cultured in DMEM medium, and bone marrow-derived dendritic cells (BMDC) were cultured in RPMI medium containing 10% FBS, 100U/mL penicillin and 100µg/mL streptomycin. Both cells were derived from wild-type (WT) and knockout (KO) mice with 20% L929-conditioned medium (LCCM) in DMEM and 20ng/mL recombinant granulocyte-macrophage colony-stimulating factor (GM-CSF) (R&D Systems, Minneapolis, MN, USA) in RPMI for BMDM and BMDC, respectively. Briefly, bone marrow cells were obtained from the femur and tibia of WT or KO mice[39]. Cells were seeded on dish plate $5x10^5$ cell/mL (day 0) and maintained in a conditioned medium and GM-CSF containing 10% FBS, 100U/mL penicillin and 100µg/mL streptomycin at 37°C, in a 5% CO_2 atmosphere for 7 days. On day 4, the medium was fully replaced, and cells were stimulated with 0.5mM PAH/Tpp Nps. As a positive control for inflammasome activation, cells were treated with 5mM Nigericin for 50min, after being primed with 1µg/mL LPS from *E. coli* (LPS E. coli) (Sigma-Aldrich, St. Louis, MO, USA) for 3h at 37°C. Supernatants were collected and cells were lysed with 25µL/well M-PERR (Thermo Fisher Scientific, Waltham, MA, USA) supplemented with 1:100 protease inhibitor cocktail (Sigma-Aldrich, St. Louis, MO, USA). Both supernatants and cell lysates were stored at −80°C until used.

Cell stimulation with Np and characterization

Flow cytometry for phenotype and cell activation characterization: BMDC were seeded in 24-well microplates at $1x10^6$ cells/well and stimulated with ultrapure 1µg/mL LPS from *E. coli* for 3h at 37°C, followed with 0.5mM PAH/Tpp Nps overnight (ON). BMDC were washed with PBS and stained for 1h at 4°C with anti-CD11c (PE), anti-CD11b (PerCP-Cy5.5), anti-MHCII (APC) and anti-CD86 (FITC) (Thermo Fisher Scientific, Waltham, MA, USA). As a positive control for inflammasome induction, cells were primed with ultrapure 1µg/mL LPS from *E. coli* for 3h, followed by 5mM ATP (Sigma-Aldrich, St. Louis, MO, USA) for 3h at 37°C. For inhibition analysis, cells were pre-treated for 30min with 100µg/mL Z-VAD-FMK (Sigma-Aldrich, St. Louis, MO, USA), 1µg/mL cytochalasin D (Santa Cruz Biotechnology Inc, Santa Cruz, CA, USA) or 50µM CA-74ME (Santa Cruz Biotechnology Inc, Santa Cruz, CA, USA) and kept in culture during the experiment. Fluorescence acquisition was performed with a FACS Aria Fusion cytometer, and data was analyzed using FlowJo software.

Reagents for inhibitions: For inhibition analysis, cells were pre-treated for 30min with 100µg/mL Z-VAD-FMK, 1µg/mL cytochalasin D or 50µM CA-74ME, 5mM 3-methyl adenine (Cayman, Ann Arbor, MI, USA) and 1 µM VPS34-IN1 (Cayman, Ann Arbor, MI, USA) and 100nM Bafilomycin A1 (Cayman, Ann Arbor, MI, USA) and kept in culture during the experiment. When indicated, at 4 hours post-Np stimulation, supernatants were removed and replaced with either complete medium or Earle's Balanced Salt Solution (EBSS) for medium starvation.

Nanoparticle internalization analysis: BMDC and BMDM were grown on glass coverslips and stimulated ON with 0.5mM FITC-PAH/Tpp Np. Poly (fluorescein isothiocyanate

allylamine hydrochloride), Mw~56000 (Sigma-Aldrich, St. Louis, MO, USA) was used instead of PAH in the PAH/Tpp formulation. Cells were fixed for 30min in 4% paraformaldehyde (PFA) at RT and nuclei were stained with 1µg/mL propidium iodide (IP) (Sigma-Aldrich, St. Louis, MO, USA). Cells were washed with PBS, blocked with 2% BSA in phosphate buffer pH=7.4 for 30min at RT and incubated with mouse anti-human LAMP1 (BD Biosciences, Franklin Lakes, NJ, USA) for 1h at RT, followed with anti-mouse Alexa 647 (Abcam, Cambridge, UK) for 1h at RT. Cells were washed, coverslips were mounted onto a slide containing 10µL of fluorescence mounting media (Dako, Abcam, Cambridge, UK) and allowed to dry at 4°C ON. Fluorescence was analyzed with a Leica SP5 Confocal Microscope.

Internalization inhibition assay: BMDC and J774 were stimulated with 0.5mM FITC-PAH/Tpp Nps and phagocytosis was inhibited with 1µg/mL cytochalasin D. Cells were characterized by flow cytometry with anti-CD11b (Percp-Cy5.5) and anti-F4/80 (APC) (Thermo Fisher Scientific, Waltham, MA, USA) and confocal microscopy for intracellular fluorescence. Nuclei were stained with 1µg/mL IP.

Intracellular immunostainings for the localization of IL-1β in autophagosomes: The J774 cell line was grown on glass coverslips and prime for 3h at 37°C with 1µg/mL LPS from E. coli, followed with 0.5mM PAH/Tpp Np for 6h. After fixation with PFA 4% for 30 min, cells were blocked with PBS-glycine (0.1 M) for 15 min, permeabilized with acetone (−20°C) for 7min, and blocked with PBS-BSA 5% for 1h at RT. Then, macrophages were incubated with the rabbit polyclonal anti-LC3B (Proteintech, Rosemont, IL, USA) and mouse polyclonal anti-IL-1β (Cell Signaling Technology, Danvers, MA, USA) in blocking buffer ON at 4°C and then incubated with the secondary anti-rabbit Alexa 594 (Abcam,

Cambridge, UK) and anti-mouse Alexa 488 (Invitrogen, Thermo Fisher Scientific, Waltham, MA, USA) antibodies for 1h at RT. Nuclei were stained with methyl green (Sigma-Aldrich, St. Louis, MO, USA) and mounted onto a slide containing fluorescence mounting media (Dako, Abcam, cambrige, UK). Image acquisition was performed with an SP5 Leica Confocal Microscope.

Epithelial cell stimulation: HT-29 cells were maintained in DMEM containing 10% FBS, 100U/mL penicillin and 100µg/mL streptomycin at 37°C with 5% CO_2, and $3x10^4$ cells/well were seeded in 96-well microplates. Cells were incubated ON to 70% confluence and the medium was fully replaced. Then, cells were stimulated ON with 0.5mM FITC-PAH/Tpp Np, or with 50ng/mL TNF-α (R&D Systems, Minneapolis, USA) for 30min at 37°C followed with FITC-PAH/Tpp Np. A mouse monoclonal anti-human EPCAM (Santa Cruz Biotechnology, Santa Cruz, CA, USA) antibody, followed bywith an anti-mouse Alexa 647 conjugated antibody (Abcam, Cambridge, UK), was used for epithelial cell detection. Cell fluorescence was analyzed with an SP5 Leica Confocal Microscope.

Inflammasome activation assessment: THP1-ASC-GFP were maintained in RPMI medium containing 10% FBS, 100U/mL penicillin and 100µg/mL streptomycin at 37°C in a 5% CO_2 atmosphere and plated at 3.6×10^5 cells/well in 96-well plates. Cells were stimulated with 0.5mM PAH/Tpp Np or primed with ultrapure 1µg/mL LPS from *E. coli* followed with 0.5mM PAH/Tpp Np ON. For a positive control, cells were primed with 1µg/mL LPS from *E. coli* for 3h and transfected with 500ng/mL bacterial plasmid cDNA. pcDNA was generated by cloning the PCR-generated full-length cDNA from a random non-related gene. Transfection was carried out with Lipofectamine™ LTX Reagent with PLUS TM Reagent (Invitrogen, Thermo Fisher Scientific, Waltham, MA, USA), following the

manufacturer´s instructions. Supernatants were harvested and stored at −80°C until used and cells were stained with DAPI (nuclear staining) (Invitrogen, Thermo Fisher Scientific, Waltham, MA, USA) and fixed with 2% PFA fixation for the microscopy analysis.

The frequency of ASC-GFP$^+$ cells and localization of fluorescent ASC specks were assessed using a Nikon Eclipse Ti Fluorescence Microscope and analyzed with ImageJ software. The total cells: ASC-GFP$^+$ cells ratio was calculated.

Quantification of secreted cytokines: Supernatants of stimulated BMDM, J774, BMDC, THP1, THP1-ASC-GFP and HT-29 cells were assessed for mIL-1β, mIL-18, mIL-6, mIFN-γ and mTNF-α using the Mouse DuoSet R&D Systems ELISA kit. The concentration of hIL-1β and hIL-8 were measured using a human Invitrogen ELISA Kit (Thermo Fisher Scientific, Waltham, MA, USA). All the protocols were used according to the manufacturer's instructions. The concentration of released LDH (enzymatic assay) (LDH-L Weiner Lab, Rosario, Santa Fe, Argentina) was quantified.

Immunoblotting analysis: Cell lysates and supernatants were analyzed by SDS-PAGE followed by immunoblotting. Proteins suspended in loading buffer (SDS+β-mercaptoethanol) were separated on a 15% SDS-PAGE gel, and transferred onto nitrocellulose membranes (Amersham Biosciences, Uppsala, Sweden) using transfer buffer (50mM Tris, 40mM glycine, 10% methanol). After blocking for 1h in TBS with 0.1% Tween-20 containing 5% non-fat dry milk, membranes were incubated overnight at 4°C with a mouse monoclonal antibody to the p20 subunit of caspase-1 (Adipogen, San Diego, CA, USA) at a 1:1,000 dilution. A loading control blot was performed with an anti–β-actin monoclonal antibody (Cell Signaling Technology, Danvers, MA, USA) at a 1:1,000 dilution. Following three washes in TBS with 0.1% Tween 20, membranes were incubated

for 1h at RT with the appropriate HRP-conjugated secondary antibody (Cell Signaling Technology, Danvers, MA, USA) at a 1:1,000 dilution. Immunoreactive bands were visualized using Luminol chemiluminescent HRP substrate (Millipore, Burlington, MA, USA) and analyzed with ImageQuant TL Software (GE Healthcare, Buckinghamshire, UK).

Analysis of the LPS content of PAH/Tpp nanoparticles

The HEK-hTLR4-reporter cell line was maintained in DMEM containing 10% FBS, 100U/mL penicillin and 100µg/mL streptomycin at 37°C with 5% CO_2. Thirty thousand cells/well were seeded in 96-well microplates and incubated to 70% confluence. The medium was fully replaced and cells were stimulated ON with different concentrations of LPS, 0.5mM PAH, 0.3mM Tpp, or 0.5mM PAH/Tpp Np. The supernatants were harvested and the secreted embryonic alkaline phosphatase (SEAP) was measured.

***In vivo* assessment of adjuvant properties**

Inflammasome characterization: Male six to nine week-old wild-type and KO C57BL/6 Nlrp3$^{-/-}$, Casp1/11$^{-/-}$, Casp11$^{-/-}$, Gsdmd$^{-/-}$ and IL-1R$^{-/-}$ mice were purchased from the Federal University of Minas Gerais and maintained under 12h cycles of light/dark. Femur and tibiae were removed for BMDM preparation and for immunization assays. Furthermore, male five to seven week-old wild-type Balb/c mice were purchased from the Laboratory of Experimental Animals, School of Veterinary Sciences of the University of La Plata (UNLP), Argentina.

Mice (C57BL/6 and Balb/c wild-type mice, and null C57BL/6 mice) were immunized once a week for three consecutive weeks intraperitoneally (IP) with OVA-conjugated PAH/Tpp Np (Np-OVA) or OVA adjuvanted with aluminum hydroxide (OVA+Alum). As a control, mice were immunized only with 100µg OVA EndoFit$^{(TM)}$. One week after the last immunization, mice were bled and sacrificed for the immune response analysis.

Humoral response assessment: OVA-specific antibodies were measured by indirect ELISA in different biological samples. Briefly, MaxiSorp plates (NUNC, Roskilde, Denmark) were coated with 1µg/mL OVA, 5mM PAH or 5mM Np in carbonate-bicarbonate buffer, pH=9.6. Coated plates were blocked with 5% equine serum in saline for 1h at 37°C, and subsequently incubated with sera (1/100) for 1h at 37°C. Bound immunoglobulins were detected with anti-mouse IgG-HRP (Biorad, Hercules, CA, USA), anti- mouse IgG1-HRP, anti-mouse IgG2a-HRP (BD Biosciences, Franklin Lakes, NJ, USA) or anti-mouse IgA-HRP (Thermo Fisher Scientific, Waltham, MA, USA). The reaction was developed with TMB (Sigma-Aldrich, St. Louis, MO, USA) and stopped with 2M H_2SO_4. OD was measured at 450 nm with Varioskan Lux (Thermo Fisher Scientific).

Assessment of secreted cytokine from stimulated splenocytes: Spleen cell suspensions were prepared in RPMI-1640 supplemented with 10% FBS, 10U/mL penicillin and 10mg/mL streptomycin, seeded ($4x10^6$ cells/mL) in culture plates and cultured for 72h at 37°C under controlled atmosphere. Cells were recalled with 10µg/mL OVA, and supernatants were harvested for mIFN-γ, mIL-5 and mIL-13 quantification by ELISA, using commercially available kits (R&D Systems, Minneapolis, MN, USA) and following the manufacturer´s instructions.

Cytokines were also assessed by intracytoplasmic flow cytometry in spleen cells. Splenocytes were incubated with brefeldin A (BD Biosciences, Franklin Lakes, NJ, USA) for the last 4h of culture and stained with anti-CD4 (PerCP-Cy5.5) anti-CD8 (APC) monoclonal Ab (Thermo Fisher Scientific, Waltham, MA, USA). Cells were fixed, permeabilized, and stained with an anti-mouse IFN-γ (FITC) (Thermo Fisher Scientific, Waltham, MA, USA). Sample acquisition was performed with a FACS Aria Fusion cytometer, and data were analyzed using the FlowJo software.

Ethics: All experimental protocols were conducted in strict agreement with international ethical standards for animal experimentation (Helsinki Declaration and its amendments, Amsterdam Protocol of Welfare and Animal Protection and National Institutes of Health, USA NIH, guidelines: Guide for the Care and Use of Laboratory Animals). Anesthetized mice (isoflurane 5%) were killed by cervical dislocation by experienced research personnel, who performed it humanely and effectively. All efforts were made to alleviate suffering during the whole experiment. All protocols were approved by the Institutional Committee for the Care and Use of Laboratory Animals of the School of Sciences (University of La Plata) (Protocol Number: 006-37-21).

Statistical analysis

All experiments were repeated at least twice with consistent outcomes. Flow cytometry data were analyzed using FlowJo X, images obtained by microscopy were analyzed using ImageJ. Graphs and data analysis were performed using GraphPad Prism8. Statistical analyses were carried out using one- or two-way ANOVA, followed by the Tukey test to discern significant differences among measurements from different experimental groups or

by the t-Student test when applicable. Quantitative data are expressed as mean ± SEM, and statistical significance was defined as $p<0.05$.

RESULTS

Phagocytic cells internalized the nanoparticles and became activated

The positively charged PAH was mixed with the negatively charged crosslinker Tpp at a ratio R=[Tpp]/[PAH]=0.6 (Figure 1A). The physicochemical properties of the self-assembled spherical nanoparticles, with a diameter of 200 nm and a negative charge potential of -23 mV, were measured using transmission electron microscopy (TEM) (Figure 1B) and dynamic light scattering (DLS) (Figure 1C)[16]. To study the interaction of PAH/Tpp Nps with cells, we exposed the murine J774 macrophages to Np. We observed the internalization and cellular distribution of fluorescent Nps by confocal microscopy after 4h of incubation. Furthermore, we did not detect any internalization of the polymer PAH-FITC (without Tpp) in macrophages (Figure S1). We observed that nanoparticles were well-dispersed into cytoplasmic vesicles (fluorescent granules) and the cytosol (diffuse fluorescence) (Figure 1D). Then, we analyzed the co-localization of the Np-FITC with LAMP1 to define the Np localization in vesicles. As it can be observed in Figure 1D, Nps were distributed between $LAMP1^{+}$- and $LAMP1^{-}$-vesicles, likely late and early endosomes (yellow and green vesicles, respectively). The incubation of cells with the inhibitor of phagocytosis cytochalasin D (Cyto D) confirmed that the internalization of Np was dependent on phagocytosis. Additionally, we detected lower fluorescence by flow cytometry in macrophages $F4/80^{+}$ $CD11b^{+}$ (Figure S1C) incubated with Cyto D than in cells exposed to Np-FITC (Figure 1E). Next, bone marrow-derived dendritic cells were

exposed to Np and LPS and we analyzed the surface expression of Class II MHC and CD86 as cell activation markers (Figure 1F). We found that BMDC expressed significantly higher levels of Class II MHC and CD86 when exposed to LPS or Np than cells exposed to nanoparticles or medium. The LPS used as a positive control for dendritic cell activation resulted in CD86 and Class II MHC expression similar to that in Np-exposed dendritic cells. These findings indicate that the cells recognized and were activated by the Np.

A similar analysis of internalization was conducted using a human intestinal epithelial cells line (HT-29). EPCAM was employed as a marker for epithelial cells, and various z-series were acquired by confocal microscopy. Neither intracellular fluorescence nor hIL-8 secretion was observed when epithelial cells were incubated with Np. Pre-activated cells with TNF-α (20ng/mL) rendered no Np up-take (Figure S2A) and production of hIL-8 (Figure S3B). As a first approach to investigate the Np-driven secretion of mIL-1β in a phagocytic cell line, we performed a LPS (1μg/mL) prime stimulus follow by a dose-response of Np. We found that 0.5mM Np promoted the highest level of secreted mIL-1β (Figure S2C).

We next investigated the production of pro-inflammatory cytokines by phagocytic cells exposed to 0.5mM of Np or controls (Figure 2). We found a significantly higher level of IL-1β in murine J774 macrophages and BMDCs, and in human THP-1 monocytes exposed to LPS+Np than cells exposed to LPS or Np (Figure 2A). We found that the different cells exposed to Np did not significantly increase IL-1β concentration compared with the medium; LPS+ATP was used as a positive control for IL-1β secretion[40]. These findings collectively suggest that Np promoted IL-1β secretion and LPS was necessary. Nevertheless, the quantification of secreted mIL-6 and hIL-8 showed no significant changes

when cells were incubated with LPS or LPS+Np, indicating that the cytokine secretion was independent of the Np presence (Figure 2B). Similarly, the cytokine levels were basal when the cells were exposed to Np (Figure 2B). Furthermore, when we analyzed mIL-18, we observed a differential secretion in J774 macrophages and BMDC incubated with LPS+Np. Cells exposed to medium, LPS or Nps showed basal levels, whereas LPS+ATP or LPS+Np induced the highest concentration of mIL-18 in BMDC (Figure 2C). These findings indicate that the secretion of IL-1β and IL-18 in APCs required LPS and Np.

Nanoparticles activated the intracellular inflammasome pathway

Inflammasomes, such as NLRP3, require the adaptor molecule ASC to activate caspase-1[41]. Following inflammasome activation, ASC assembles into a large protein complex, which can be visualized as a "speck"[42]. Representative pictures are shown with white arrowheads indicating GFP-specks (Figure 3A). The number of specks in LPS+Np-treated cells was significantly higher ($p \leq 0.05$) than in cells exposed to medium or LPS and equal to the positive control with LPS+DNA (Figure 3B). This finding suggests that Np triggered the assembly of the ASC complex. A similar analysis was performed using flow cytometry to quantify ASC^+ cells[43], and it was observed that cells exposed to LPS+DNA or LPS+Np had a significantly higher frequency of ASC^+ cells compared to resting cells (Figure 3C and D). The ratio of GFP-ASC^+ cells:total cells triggered by Np was similar to the positive control condition of LPS+DNA. Additionally, the quantification of hIL-1β in the supernatants showed that LPS+DNA or LPS+Np induced higher levels of this cytokine than medium or LPS ($p<0.05$) (Figure 3E). To investigate the inflammasome activation, we used different pathway inhibitors. We found that cytochalasin D, the cathepsin B inhibitor CA-074Me and

the caspase-1 inhibitor Z-VAD-FMK significantly suppressed the mIL-1β secretion induced by LPS+Np ($p<0.001$) (Figure 3F). The analysis of the mIL-18 secretion showed similar results, with a higher secretion in cells exposed to LPS+Np than in cells incubated with LPS or medium, and the inhibitors suppressed the cytokine secretion (Figure 3F). Our results suggest that Np promoted inflammasome activation through cathepsin B and caspase-1. These findings led us to perform an experiment using inflammasome-null mice for NLRP3, caspase-1/11, caspase-11 and gasdermin D (GSDMD). BMDM obtained from NLRP3$^{-/-}$, caspase1/11$^{-/-}$, caspase11$^{-/-}$ and GSDMD$^{-/-}$ mice were incubated with 1μg/mL LPS and 0.5mM of Np. To analyze the inflammasome activation, we quantified secreted mIL-1β and mTNF-α by ELISA in the supernatants. We observed no mIL-1β secretion in cells stimulated with LPS or Np in wild-type and KO mice. However, exposure to LPS+Np induced the production and release of this cytokine in wild-type, caspase11$^{-/-}$ and GSDMD$^{-/-}$ BMDM. In contrast, cells from NLRP3$^{-/-}$ and caspase1/11$^{-/-}$ mice showed decreased mIL-1β secretion compared to wild-type animals ($p<0.001$) (Figure 4A). When the BMDM WT and caspase11$^{-/-}$ were stimulated with the positive control LPS+Nigericin, we detected the production of IL-1β. Meanwhile, the secretion of IL-1β in BMDM from NLRP3$^{-/-}$, caspase1$^{-/-}$ and GSDMD$^{-/-}$ was significantly abrogated (Figure 4A). The quantification of soluble mTNF-α showed that cells from wild-type and KO mice secreted similar high amounts upon exposure to LPS, LPS+Np or LPS+Nigericin. No TNF- α was induced when cells were incubated with Np (Figure 4B). LDH measured in the supernatants showed that the stimuli did not significantly affect the cells. The consistent level of soluble LDH in cells exposed to the medium, Np or LPS+Np indicated that cell viability was unaffected (Figure S3A). Additionally, the lysate of LPS+Np-exposed cells from wild-type or KO mice showed a minimal difference in the activation of caspase-1 (20 kDa) between cells derived

from wild-type and NLRP3$^{-/-}$ mice. Inactive caspase-1 was detected in resting and LPS+Np-stimulated cells, while it was absent in samples from cells of caspase1/11$^{-/-}$ animals (Figure S3B).

As mentioned before, we found that the release of mIL-1β was independent of GSDMD (Figure 4A). This prompted us to study the secretion of IL-1β and IL-18. Among the multiple pathways described in myeloid cells, we investigated autophagy as responsible for the secretion of IL-1β. As starvation has been reported to induce autophagy[44,45], we performed experiments using the EBSS starvation medium following cell activation. We observed a significant increase in the production of mIL-1β when macrophages were stimulated with LPS+Np and supplemented with EBSS medium compared to the cells that were stimulated with LPS+Np (Figure 4C). To confirm this finding, we used 3-methyladenine (3-MA) (blocker of early stages of autophagy) and VPS34-IN1 (inhibitor of the class III PI3K) as autophagy inhibitor. All treatments significantly decreased the mIL-1β secretion in cells exposed to LPS+Np (Figure 4D). To confirm if autophagy is involved in the secretion of mIL-1β, we measured a pro-inflammatory cytokine (mIL-6) that is release through the canonical ER-Golgi and autophagy-independent pathway. We observed unchanged high levels of mIL-6 in cells exposed to LPS+Np irrespective of the presence of EBSS (Figure S3C). However, when the different inhibitory conditions were assessed, we found that 3-MA led to a not significantly decreased cytokine level (Figure S3D). Nevertheless, it is essential to note that this effect was negligible compared to that exerted on mIL-1β secretion (Figure 4D). Additionally, we did not observe a significant increase in the release of LDH in the cells, either with or without the autophagy inhibitors (Figure S3E). Moreover, we observed the same results in BMDCs: the release of IL-1β was

abrogated after the treatment with the autophagy inhibitors (Figure S3F). Finally, we found by confocal microscopy that mIL-1β co-localized with LC3B, a central protein in the autophagy pathway and autophagosome biogenesis, when macrophages were stimulated with LPS+Np (Figure 4E) compared to cells incubated with medium, Np or LPS (Figure S3G).

Overall, these findings confirmed that the NLRP3-dependent inflammasome pathway was involved in cell activation with IL-1β production, and that autophagy was involved in the secretion of IL-1β induced by LPS+Np. However, considering the reduced level of mIL-1β in cells from NLRP3$^{-/-}$ mice compared with wild-type animals and the active caspase-1 observed in lysates of NLRP3$^{-/-}$ cells (Figure S3B), we suggest that an NLRP3-independent inflammasome pathway may also be involved in mIL-1β production. Besides, the consistent level of soluble LDH in cells exposed to the medium, Np or LPS+Np indicated that cell viability was unaffected upon activation.

The systemic administration of Np-OVA triggered a specific humoral and cellular immune response

To characterize its adjuvanticity *in vivo*, we first measured the presence of LPS in PAH, Tpp and Np with the human TLR4 HEK reporter cells and secreted SEAP, as readout. We found that the SEAP activity were comparable to that in non-stimulated cells and lower than 0.01 ng/mL of LPS (Figure S4). The percentage of OVA encapsulation by Np depends on the final concentration, with a higher yield obtained at a concentration of 100µg/mL (Figure S5).

Then, mice were intraperitoneally injected with Np-OVA in 3 weekly doses (Figure. 5A). As a control, we administered a formulation containing the approved adjuvant for human use, aluminum hydroxide (Alum)[46], with OVA. No weight loss was observed during the whole experiment in mice (Figure 5B). We did not observe specific antibodies to the nanoparticle or the polymer PAH in animals immunized with Np-OVA (Figure 5C). Animals that received Np-OVA produced higher levels of serum OVA-specific IgG than mice injected with OVA ($p<0.01$) and similar values compared with mice that received OVA+Alum (Figure. 5D). The subclass analysis revealed that Np-OVA induced higher titers of OVA-specific IgG2a than in mice injected with OVA+Alum (Figure 5E); in addition, the ratio of IgG subclasses in Np-OVA and OVA+Alum injected mice showed a higher production of OVA-specific IgG2a in Np-OVA immunized animals (Figure 5F). To analyze the T cell-mediated immune response, spleen cells from mice immunized with Np-OVA, OVA+Alum and OVA were stimulated with OVA and cytokines were measured in the supernatants. We found that mice immunized with Np-OVA induced increased levels of IFN-γ when cells were stimulated with OVA ($p<0.001$). Cells from mice that received OVA or OVA+Alum did not secrete IFN-γ (Figure 5F). On the other hand, the Th2 cytokines mIL-5 and mIL-13 showed decreased concentration in the Np-OVA treated mice as compared to mice administered with OVA+Alum (Figure 5F). To further evaluate the cell source of IFN-γ, spleen cells were analyzed by intracellular cytokine staining following *in vitro* OVA stimulation. We found that the frequency of $CD4^+IFN\text{-}\gamma^+$ and $CD8^+IFN\text{-}\gamma^+$ lymphocytes was significantly increased in mice immunized with Np-OVA (Figure 5G and H). Overall, these findings support that Np-OVA promoted the induction of a Th1-dependent immune response with specific IgG and IgG2a, and $CD4^+IFN\text{-}\gamma^+$ and $CD8^+IFN\text{-}\gamma^+$ T cells following the immunization with OVA adjuvanted with Np.

To investigate the role of the inflammasome pathway in promoting the specific immune response, C57BL/6 mice wild-type and NLRP3$^{-/-}$, caspase1/11$^{-/-}$ and IL-1R$^{-/-}$ mice were intraperitoneally immunized with Np-OVA. As shown in Figure 6A, NLRP3$^{-/-}$ and caspase1/11$^{-/-}$ mice exhibited lower levels of serum OVA-specific IgG than wild-type mice ($p<0.01$), whereas IL1-R null mice showed similar levels than wild-type mice (Figure 6A). Finally, spleen cells from wild-type and KO mice were stimulated with OVA or medium, and IFN-γ levels were assessed in the supernatants. We found that cells from wild-type mice sensitized with Np-OVA showed higher levels of IFN-γ than cells from WT mice sensitized with OVA, and NLRP3$^{-/-}$ and caspase1/11$^{-/-}$ mice sensitized with Np-OVA. Cells from IL1-R$^{-/-}$ mice sensitized with Np-OVA showed a similar concentration of IFN-γ to WT animals (Figure 6B). These findings showed that the NLRP3 pathway was critical to promoting the OVA-specific Th1-dependent immune response.

DISCUSSION

Our findings showed that Np are exclusively internalized by phagocytic antigen-presenting cells, specifically dendritic cells and macrophages. Subsequently, they localize intracellularly within the endosome compartment, causing their disruption and leading to the translocation of their components into the cytosol. Thus, the internalization of Np triggers the cellular activation and inflammasome assembly, releasing the pro-inflammatory cytokines IL-1β and IL-18 to the extracellular medium. Remarkably, we did not observe the Np internalization in non-phagocytic mucosa epithelial cells. The permeabilization of the lysosomal membrane is one of the most frequently described mechanisms for activating the inflammasome by particles and Np[47,48]. We used several inhibitors to confirm the role of the different components of the pathway, and we corroborated the participation of cathepsin B as the early activator of the inflammasome[49,50]. Then, using BMDM KO for receptors and enzymes involved in this pathway, we confirmed that cellular activation depended on the NLRP3 receptor and caspase-1 but not on caspase-11. These findings demonstrate that the Np activates the NLRP3 inflammasome through the canonical pathway. Nevertheless, we found that the release of IL-1β was independent of gasdermin D pores, which is associated with the slow release of the cytokine and the absence of cellular death by pyroptosis[51]. The literature shows that the non-canonical autophagy pathway is involve in the secretion of inflammatory molecules such as IL-1β and HMGB1[52,53]. In macrophages and monocytes, LC3B is essential for the efficient secretion of IL-1β in response to lysosomal damage[45,54]. In this sense, we demonstrated that the inflammasome activation proceeded with autophagy induction for secreting IL-1β. All together these findings demonstrated that PAH-based Np activated phagocytic cells with increased expression of MHC II and CD86, along with the

secretion of IL-1β and IL-18, without inducing cell death, which make them a candidate adjuvant to trigger an antigen-specific immune response.

It is known that aluminum salts, such as the extensively used in human vaccines aluminum hydroxide (alum), can enhance the effectiveness of the immune response by activating antigen-presenting cells through the depot effect and the aggregation of antigens to improve the uptake and activation of APCs. Furthermore, it has been described that alum triggered the NLRP3-dependent inflammasome pathway to further promote adaptive immunity and memory[55]. Thus, we evaluated the *in vivo* adjuvant capacity of PAH/Tpp Np in mice that were systemically administered with OVA encapsulated in Np. We observed the induction of innate immunity via the inflammasome-dependent pathway to further promote a Th1-driven adaptive humoral and cellular immunity. Our findings showed the induction of serum IgG and IgG2a-specific antibodies, and the expansion of $CD4^+$- and $CD8^+$-IFN-γ-producing T cells. Furthermore, we confirmed *in vivo* that the Th1-dependent isotype synthesis and IFN-γ production were NLRP3- and caspase-1-dependent. It is reported that the NLRP3 inflammasome pathway initiates a caspase-1–dependent IL-1β and IL-18 secretion promoting interferon-γ production and Th1 differentiation[56,57]. Similar to other adjuvants, such as Alum and QS-21, PAH-based nanoparticles along with LPS as a first inflammasome activation signal induced *in vitro* the NLRP3-ASC-caspase-dependent IL-1β production. *In vivo*, however, the first signal may be triggered by a DAMP, such as uric acid, generated at the immunization site[58,59]. Additionally, IL-18, constitutively expressed by several cell types, can stimulate IL-1β transcription and may initiate a pro-inflammatory cascade during vaccination[60]. The *in vivo* induction of OVA-specific $CD8^+$T cells indicates that Np-OVA triggered the cross-presentation of OVA, which may proceed upon the

endosome is disrupted and the content is translocated into the cytosol. Further studies are needed to confirm if macrophages and dendritic cells contribute to this mechanism, which is critical when considering using PAH-based Np as an adjuvant in an anti-tumoral or viral vaccine.

Muñoz-Wolf et al. reported that polymeric nanoparticles made of poly-lactic-co-glycolic acid with a diameter of 50-60nm elicited a robust cellular immune response through the caspase-11- and the pyroptosis effector gasdermin D-dependent non-canonical inflammasome pathway. They described a division of labor for IL-1β and IL-18 to induce the appropriate immunogenic context for Th1 and $CD8^+$ T cell induction, respectively[61]. In our study, we characterized a polymeric nanoparticle of PAH that activated murine and human macrophages and dendritic cells through the canonical caspase-1- and NLRP3-dependent inflammasome pathway with the secretion of IL-1β and IL-18, without cell death, and independent of caspase-11 and gasdermin D-dependent pyroptosis[62,63]. We found that PAH-based Np induced autophagy for the secretion of the pro-inflammatory cytokine IL-1β.

In conclusion, we characterized a novel polyallylamine-based self-assembled nanoparticle as a systemic safe adjuvant that targeted the encapsulated OVA immunogen to phagocytic cells, endowing these antigen-processing cells with T cell activation capacity that triggered a Th1-dependent humoral and cellular immune response. These findings may pave the way for designing and developing novel nanoparticle-based systemic vaccines for infectious and non-infectious diseases.

CONFLICT OF INTEREST

None of the authors has a financial, commercial or personal relationship that could inappropriately influence or bias the content of the paper.

AUTHOR CONTRIBUTIONS

GPR Conceptualization, Data curation, Formal analysis, Investigation, Methodology, Visualization, Writing – original draft, Writing – review & editing**.** *RCS* Data curation, Methodology. *CC* Data curation, Formal analysis, Investigation, Methodology**.** *DB* Data curation, Formal analysis, Investigation, Methodology**.** *EA* Data curation, Methodology**.** *SEH* Data curation, Methodology, Writing – original draft, Writing – review & editing**.** *MLA* Data curation, Methodology**.** IK Formal analysis, Methodology, Writing-review & editing. AT Formal analysis, Methodology, Writing-review & editing. *SCO* Supervision, Visualization, Writing – original draft, Writing – review & editing**.** *OA* Supervision, Visualization, Writing – original draft, Writing – review & editing**.** *PLS* Conceptualization, Data curation, Formal analysis, Funding acquisition, Investigation, Methodology, Supervision, Visualization, Writing – original draft, Writing – review & editing**.** *GHD* Conceptualization, Formal analysis, Funding acquisition, Investigation, Supervision, Visualization, Writing – original draft, Writing – review & editing.

FUNDINGS

This research was supported by grants from the Universidad Nacional de La Plata [UNLP, grant No. 11/X695] and the Agencia Nacional de Promoción Científica y Tecnológica [ANPCyT, grant No. PICT 2019-0368 and 2020-3166] to PLS and GHD, Fundação de Amparo à Pesquisa do Estado de São Paulo (FAPESP) grant No 2023/02577-5 to SCO and National Institutes of Health (NIH) grant No R01 AI116453

ACKNOWLEDGMENTS

SHE, MLA, AT, OA, PLS and GHD are researchers of CONICET; RCS and SCO are researchers of *Federal University of Minas Gerais and University of São Paulo; GPR, DB, EA and IK are* fellows of CONICET; CC is fellow of ANPCyT.

REFERENCES

1. Zhao, L. *et al.* Nanoparticle vaccines. *Vaccine* **32**, 327–337 (2014).

2. Irvine, D. J. & Read, B. J. Shaping humoral immunity to vaccines through antigen-displaying nanoparticles. *Curr. Opin. Immunol.* **65**, 1–6 (2020).

3. Huang, M., Zhang, M., Zhu, H., Du, X. & Wang, J. Mucosal vaccine delivery: A focus on the breakthrough of specific barriers. *Acta Pharm. Sin. B* **12**, 3456–3474 (2022).

4. Walls, A. C. *et al.* Elicitation of Potent Neutralizing Antibody Responses by Designed Protein Nanoparticle Vaccines for SARS-CoV-2. *Cell* **183**, 1367-1382.e17 (2020).

5. Arunachalam, P. S. *et al.* Adjuvanting a subunit COVID-19 vaccine to induce protective immunity. *Nature* **594**, 253–258 (2021).

6. Dalvie, N. C. *et al.* Engineered SARS-CoV-2 receptor binding domain improves manufacturability in yeast and immunogenicity in mice. *Proc. Natl. Acad. Sci. U. S. A.* **118**, (2021).

7. Herrera, S. E. *et al.* Polyelectrolyte-multivalent molecule complexes: physicochemical properties and applications. *Soft Matter* (2023) doi:10.1039/d2sm01507b.

8. Herrera, S. E. *et al.* Polyelectrolyte–Ion Complexes as Stimuli-Responsive Systems for Controlled Drug Delivery. in *Supramolecular Nanotechnology* 729–764 (John Wiley & Sons, Ltd, 2023). doi:https://doi.org/10.1002/9783527834044.ch27.

9. Lawrence, P. G., Patil, P. S., Leipzig, N. D. & Lapitsky, Y. Ionically Cross-Linked Polymer Networks for the Multiple-Month Release of Small Molecules. *ACS Appl. Mater. Interfaces* **8**, 4323–4335 (2016).

10. Goldsmith, D. R., Scott, L. J., Cvetković, R. S. & Plosker, G. L. Sevelamer hydrochloride: A review of its use for hyperphosphataemia in patients with end-stage renal disease on haemodialysis. *Drugs* **68**, 85–104 (2008).

11. Aoyama, S., Matsumoto, Y., Mori, C. & Sota, K. Application of novel mixed mode chromatography (MMC) resins having a hydrophobic modified polyallylamine ligand for monoclonal antibody purification. *J. Chromatogr. B* **1191**, 123072 (2022).

12. Chang, Y. C. *et al.* Rapid detection of gut microbial metabolite trimethylamine n-oxide for chronic kidney disease prevention. *Biosensors* **11**, (2021).

13. Herrera, S. E. *et al.* Layer-by-Layer Formation of Polyamine-Salt Aggregate/Polyelectrolyte Multilayers. Loading and Controlled Release of Probe Molecules from Self-Assembled Supramolecular Networks. *Macromol. Chem. Phys.* **220**, 1–10 (2019).

14. Cuenca, V. E. *et al.* Polyphosphate Poly(amine) Nanoparticles: Self-Assembly, Thermodynamics, and Stability Studies. *Langmuir* **35**, 14300–14309 (2019).

15. Bugnicourt, L. & Ladavière, C. Interests of chitosan nanoparticles ionically cross-linked with tripolyphosphate for biomedical applications. *Prog. Polym. Sci.* **60**, 1–17 (2016).

16. E. Apuzzo, M. Agazzi, S. Herrera, A. Picco, G. Rizzo, C. Chavero, D. Bianchi, P. Smaldini, L. Cortez, W. Marmisollé, G. Padula, A. Seoane, M. Alomar, M.

Denofrio, G. Docena, O. A. Poly (allylamine) -tripolyphosphate ionic assemblies as nanocarriers : friend or foe? (2023) doi:10.1021/acsabm.3c00489.

17. Boraschi, D. *et al.* Nanoparticles and innate immunity: new perspectives on host defence. *Semin. Immunol.* **34**, 33–51 (2017).

18. Jo, E. K., Kim, J. K., Shin, D. M. & Sasakawa, C. Molecular mechanisms regulating NLRP3 inflammasome activation. *Cell. Mol. Immunol.* **13**, 148–159 (2016).

19. Lei, H. *et al.* Cationic nanocarriers as potent adjuvants for recombinant S-RBD vaccine of SARS-CoV-2. *Signal Transduct. Target. Ther.* **5**, 4–6 (2020).

20. Zhao, L., Skwarczynski, M. & Toth, I. Polyelectrolyte-Based Platforms for the Delivery of Peptides and Proteins. *ACS Biomater. Sci. Eng.* **5**, 4937–4950 (2019).

21. Malik, A., Gupta, M., Gupta, V., Gogoi, H. & Bhatnagar, R. Novel application of trimethyl chitosan as an adjuvant in vaccine delivery. *Int. J. Nanomedicine* **13**, 7959–7970 (2018).

22. Fadeel, B. Clear and present danger ? Engineered nanoparticles and the immune system. 1–9 (2012) doi:10.4414/smw.2012.13609.

23. Kawai, T. & Akira, S. The role of pattern-recognition receptors in innate immunity : update on Toll-like receptors. *Nat. Publ. Gr.* **11**, 373–384 (2010).

24. Iwasaki, A. & Medzhitov, R. Control of adaptive immunity by the innate immune system. **16**, 343–353 (2015).

25. Martinon, F., Burns, K. & Tschopp, J. The Inflammasome: A molecular platform triggering activation of inflammatory caspases and processing of proIL-β. *Mol. Cell*

10, 417–426 (2002).

26. Serrano-Puebla, A. & Boya, P. Lysosomal membrane permeabilization in cell death: new evidence and implications for health and disease. *Ann. N. Y. Acad. Sci.* **1371**, 30–44 (2016).

27. Campden, R. I. & Zhang, Y. The role of lysosomal cysteine cathepsins in NLRP3 inflammasome activation. *Arch. Biochem. Biophys.* **670**, 32–42 (2019).

28. Zhivaki, D. *et al.* Inflammasomes within Hyperactive Murine Dendritic Cells Stimulate Long-Lived T Cell-Mediated Anti-tumor Immunity. *Cell Rep.* **33**, 108381 (2020).

29. Evavold, C. L. *et al.* The Pore-Forming Protein Gasdermin D Regulates Interleukin-1 Secretion from Living Macrophages. *Immunity* **48**, 35-44.e6 (2018).

30. Monteleone, M. *et al.* Interleukin-1β Maturation Triggers Its Relocation to the Plasma Membrane for Gasdermin-D-Dependent and -Independent Secretion. *Cell Rep.* **24**, 1425–1433 (2018).

31. Saeki, A. *et al.* Gasdermin D-independent release of interleukin-1β by living macrophages in response to mycoplasmal lipoproteins and lipopeptides. *Immunology* **161**, 114–122 (2020).

32. Brubaker, S. W., Bonham, K. S., Zanoni, I. & Kagan, J. C. *Innate Immune Pattern Recognition : A Cell Biological Perspective*. (2015). doi:10.1146/annurev-immunol-032414-112240.

33. Qu, Y., Franchi, L., Nunez, G. & Dubyak, G. R. Nonclassical IL-1β Secretion

Stimulated by P2X7 Receptors Is Dependent on In?ammasome Activation and Correlated with Exosome Release in Murine Macrophages. (2015) doi:10.4049/jimmunol.179.3.1913.

34. Abu Khweek, A. & Amer, A. O. Pyroptotic and non-pyroptotic effector functions of caspase-11. *Immunol. Rev.* **297**, 39–52 (2020).

35. Kayagaki, N. *et al.* Non-canonical inflammasome activation targets caspase-11. *Nature* **479**, 117–121 (2011).

36. Bourque, J. & Hawiger, D. *Immunomodulatory bonds of the partnership between dendritic cells and T cells*. *Critical Reviews in Immunology* vol. 38 (2018).

37. Reddy, S. T., Swartz, M. A. & Hubbell, J. A. Targeting dendritic cells with biomaterials: developing the next generation of vaccines. *Trends Immunol.* **27**, 573–579 (2006).

38. Babensee, J. E. Interaction of dendritic cells with biomaterials. *Semin. Immunol.* **20**, 101–108 (2008).

39. Weischenfeldt, J. & Porse, B. Bone marrow-derived macrophages (BMM): Isolation and applications. *Cold Spring Harb. Protoc.* **3**, 1–7 (2008).

40. Cullen, S. P., Kearney, C. J., Clancy, D. M. & Martin, S. J. Diverse Activators of the NLRP3 Inflammasome Promote IL-1β Secretion by Triggering Necrosis. *Cell Rep.* **11**, 1535–1548 (2015).

41. Chan, A. H. & Schroder, K. Inflammasome signaling and regulation of interleukin-1 family cytokines. *J. Exp. Med.* **217**, 1–10 (2020).

42. Hoss, F., Rodriguez-Alcazar, J. F. & Latz, E. Assembly and regulation of ASC specks. *Cell. Mol. Life Sci.* **74**, 1211–1229 (2017).

43. Sester, D. P. *et al.* A Novel Flow Cytometric Method To Assess Inflammasome Formation. *J. Immunol.* **194**, 455–462 (2015).

44. Iula, L. *et al.* Autophagy mediates interleukin-1β secretion in human neutrophils. *Front. Immunol.* **9**, 1–14 (2018).

45. Dupont, N. *et al.* Autophagy-based unconventional secretory pathway for extracellular delivery of IL-1β. *EMBO J.* **30**, 4701–4711 (2011).

46. Kwissa, M., Kasturi, S. P. & Pulendran, B. The science of adjuvants. *Expert Rev. Vaccines* **6**, 673–684 (2007).

47. Hornung, V. *et al.* Silica crystals and aluminum salts activate the NALP3 inflammasome through phagosomal destabilization. *Nat. Immunol.* **9**, 847–856 (2008).

48. Ma, L. *et al.* Characterization of Cathepsin B in Mediating Silica Nanoparticle-Induced Macrophage Pyroptosis via an NLRP3-Dependent Manner. 4537–4545 (2022).

49. Chevriaux, A. *et al.* Cathepsin B Is Required for NLRP3 Inflammasome Activation in Macrophages, Through NLRP3 Interaction. *Front. Cell Dev. Biol.* **8**, 1–8 (2020).

50. Sahoo, M., Ceballos-Olvera, I., Del Barrio, L. & Re, F. Role of the inflammasome, IL-1β, and IL-18 in bacterial infections. *ScientificWorldJournal.* **11**, 2037–2050 (2011).

51. Baroja-Mazo, A. *et al.* Early endosome autoantigen 1 regulates IL-1β release upon caspase-1 activation independently of gasdermin D membrane permeabilization. *Sci. Rep.* **9**, 1–10 (2019).

52. Ponpuak, M. *et al.* Secretory autophagy. *Curr. Opin. Cell Biol.* **35**, 106–116 (2015).

53. Deretic, V. Autophagy in inflammation, infection, and immunometabolism. *Immunity* **54**, 437–453 (2021).

54. Kimura, T. *et al.* Dedicated SNARE s and specialized TRIM cargo receptors mediate secretory autophagy . *EMBO J.* **36**, 42–60 (2017).

55. Sweatt,S.K, Gower, B.A, Chieh, A.Y, Liu, Y, Li, L. Crucial role for the Nalp3 inflammasome in the immunostimulatory properties of aluminium adjuvants. *Physiol. Behav.* **176**, 139–148 (2016).

56. Daniel E Shumer, Natalie J Nokoff, N. P. S. & Erin C. Dowd, M.D.a, Michael J. Frank, Ph.D.b, Anne Collins, Ph.D.c, James M. Goldd, and Deanna M. Barch, P. D. . T helper 1 immunity requires complement-driven NLRP3 inflammasome activity in CD4+ T cells. *Physiol. Behav.* **176**, 139–148 (2017).

57. Wagatsuma, K. & Nakase, H. Contradictory effects of NLRP3 inflammasome regulatory mechanisms in colitis. *Int. J. Mol. Sci.* **21**, 1–24 (2020).

58. Marty-Roix, R. *et al.* Identification of QS-21 as an inflammasome-activating molecular component of saponin adjuvants. *J. Biol. Chem.* **291**, 1123–1136 (2016).

59. Kool, M. *et al.* Alum adjuvant boosts adaptive immunity by inducing uric acid and activating inflammatory dendritic cells. *J. Exp. Med.* **205**, 869–882 (2008).

60. Content, R. Alum ’ s Adjuvant Effect Are Mediated by NLRP3 1. **181**, 17–21 (2014).

61. Muñoz-Wolf, N. *et al.* Non-canonical inflammasome activation mediates the adjuvanticity of nanoparticles. *Cell Reports Med.* **4**, (2023).

62. Kaplanski, G. Interleukin-18: Biological properties and role in disease pathogenesis. *Immunol. Rev.* **281**, 138–153 (2018).

63. Lacaille-Dubois, M. A. Updated insights into the mechanism of action and clinical profile of the immunoadjuvant QS-21: A review. *Phytomedicine* **60**, 152905 (2019).

FIGURES

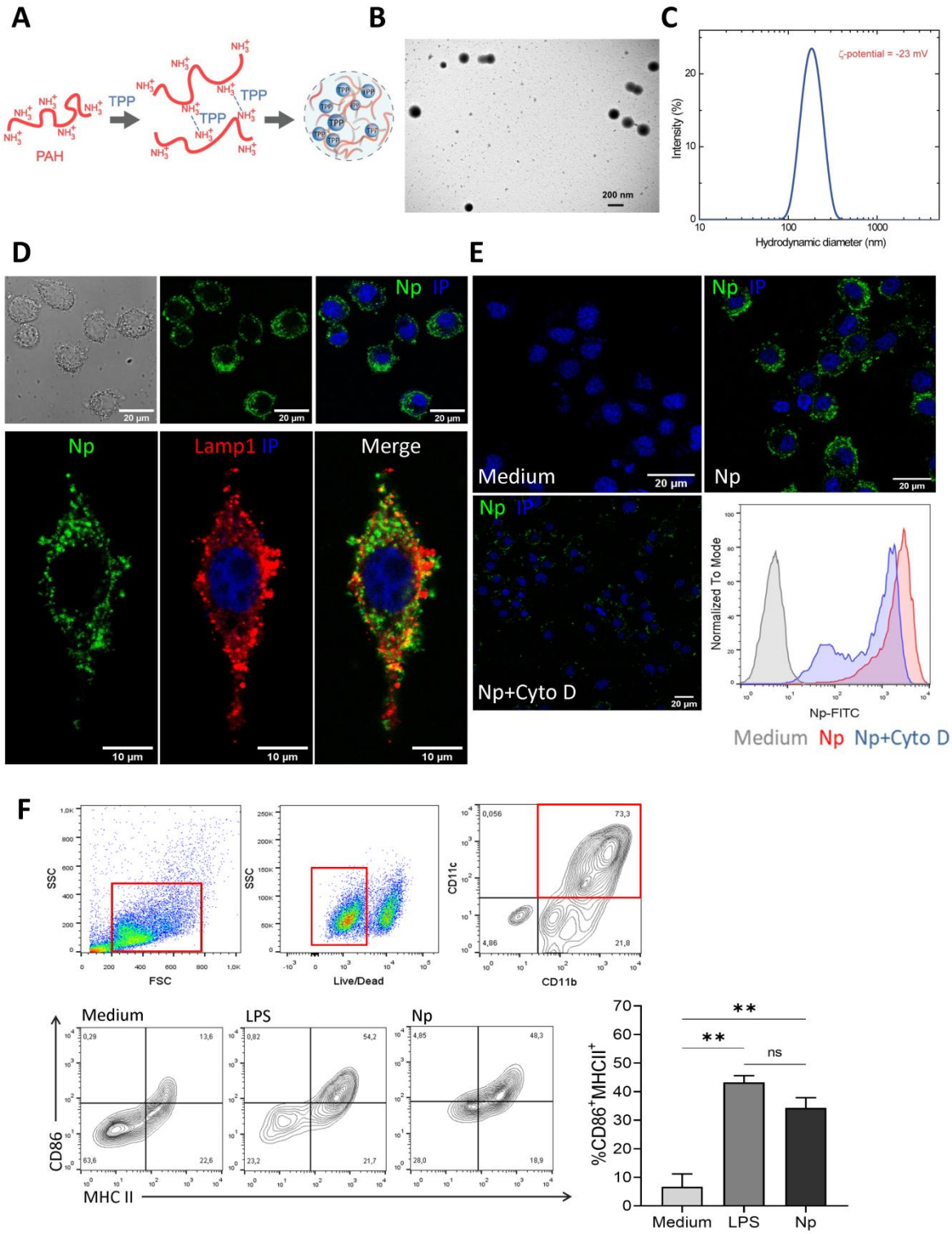

Figure 1: Cell uptake of Np and activation. (A) Schematic Np composition; **(B)** TEM image of the Np prepared at a Tpp/PAH=0.6 ratio; **(C)** Particle size measured by DLS. **(D)**

Np-FITC internalized by J774 and colocalization with the late endosome marker LAMP-1 by confocal microscopy after 4h stimulation. **(E)** Inhibition of phagocytosis of Np-FITC with cytochalasin D in BMDM by confocal microscopy and flow cytometry. **(F)** BMDC surface expression of CD86 and MHCII in BMDC ($CD11b^{+}CD11c^{+}$) by flow cytometry. All experiments were performed in triplicate and data are expressed as mean±SEM. P-value was determined by ordinary one-way ANOVA *P<0,05; **P<0,01.

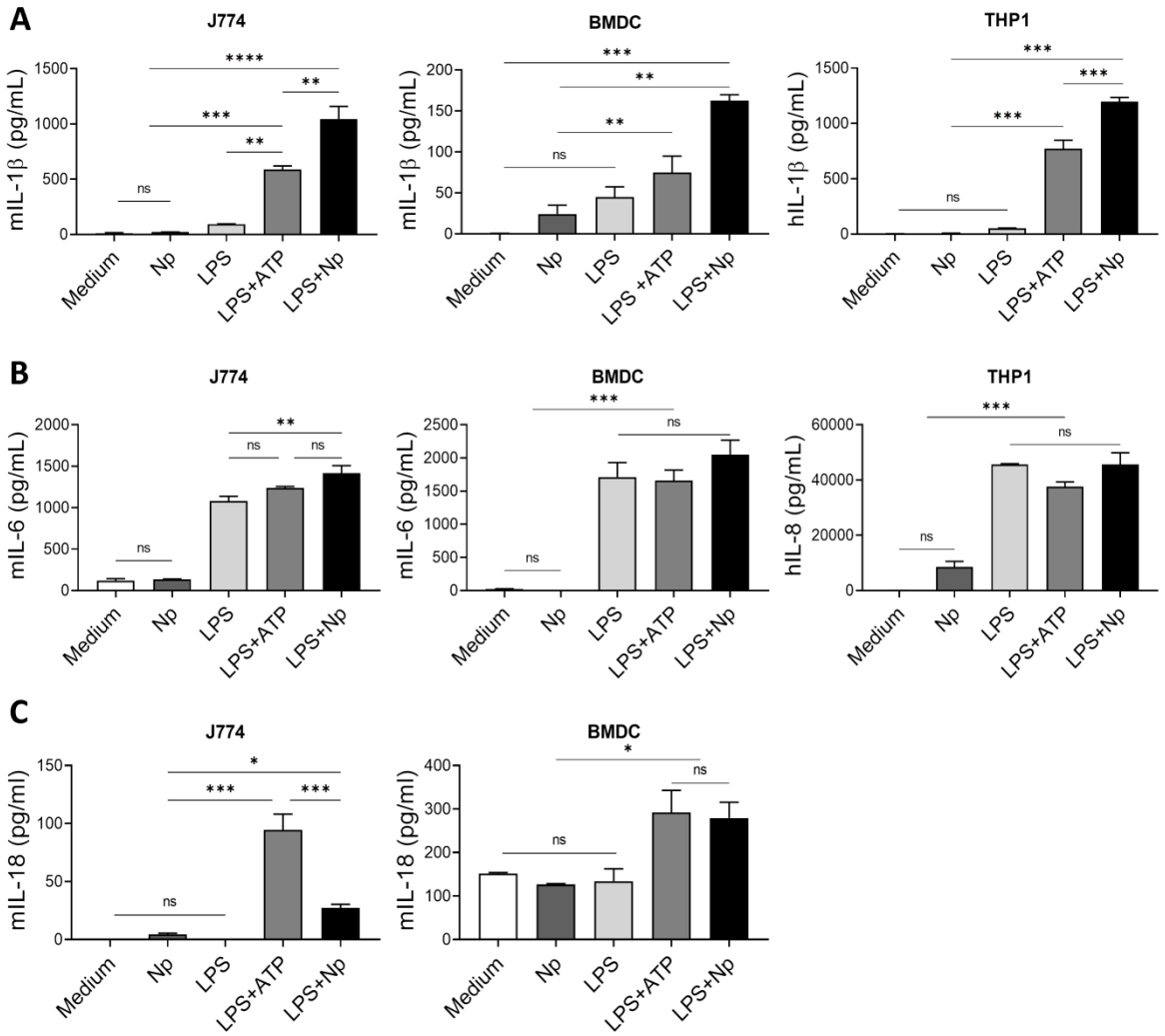

Figure 2: Secretion of pro-inflammatory cytokine by macrophages, dendritic cells and monocytes. J774, THP-1 and BMDC were prime with LPS (1µg/mL) for 3h; the medium

was fully replaced and stimulated with ATP (50nM) for 3h as a positive control or with Np (0.5mM) overnight. Controls of LPS and Np were stimulated overnight. **(A)** IL-1β and **(B)** IL-6 and IL-8 and **(C)** IL-18 secreted cytokine by phagocyte cells were measured in supernatants by ELISA. All experiments were carried out in triplicate and date are expressed as mean±SEM. P-value was determined by ordinary One-way ANOVA *P<0,05; **P<0,01; ***P<0,001; ****p<0,0001.

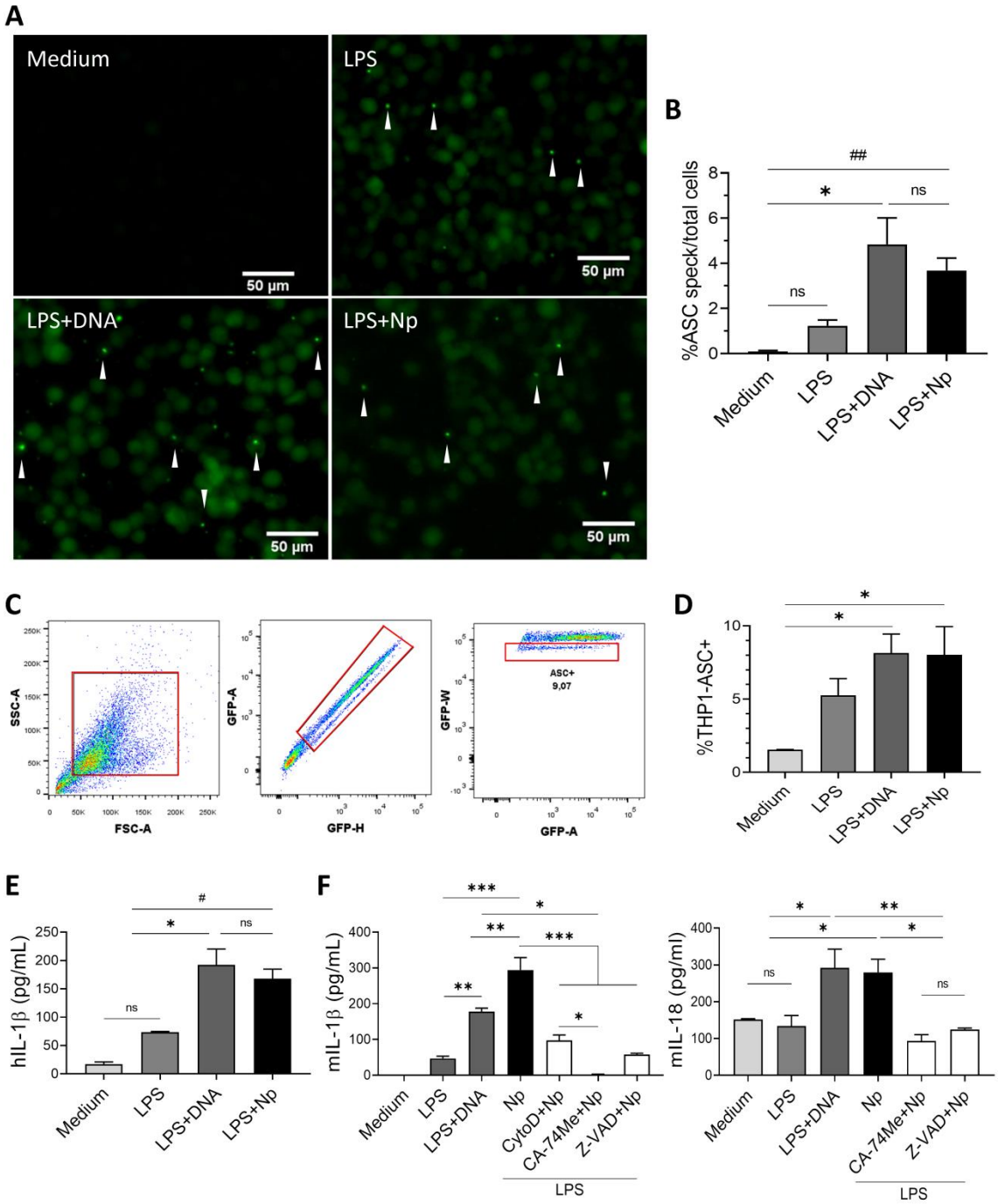

Figure 3: Inflammasome activation and cytokine secretion in THP1-ACS-GFP cells. Cells were primed with LPS for 3 hours. The medium was fully replaced, and the cells were either stimulated with Np overnight or transfected with pcDNA as positive controls. **(A)** ASC-GFP speck within the cells are shown with white arrow, performed by

epifluorescence microscopy; **(B)** Frequency of speck ASC-GFP^{+}cells. Three independent experiments were performed. Each bar represents the average number of total speck^{+} cells/total cells per field; 3 fields for each treatment were counted (2 replicates/treatment); **(C)** Flow cytometry gate strategy to define ASC-GFP^{+}cells; **(D)** Frequency of speck ASC-GFP^{+}cells by flow cytometry; **(E)** Quantification of secreted hIL-1β by ELISA. **(F)** BMDC were stimulated overnight with LPS+Np and simultaneously inhibited with cytochalasin D for phagocytosis, CA-74Me for cathepsin B and Z-VAD-FMK (Z-VAD) for caspase-1 during 30min, and quantification of secreted mIL-1β and mIL-18 by ELISA. All experiments were carried out in triplicate and date are expressed as mean±SEM. P-value was determined by ordinary one-way ANOVA *p<0,05; **p<0,01; ***p<0,001 or t-Student #p<0,05; ##p<0,01.

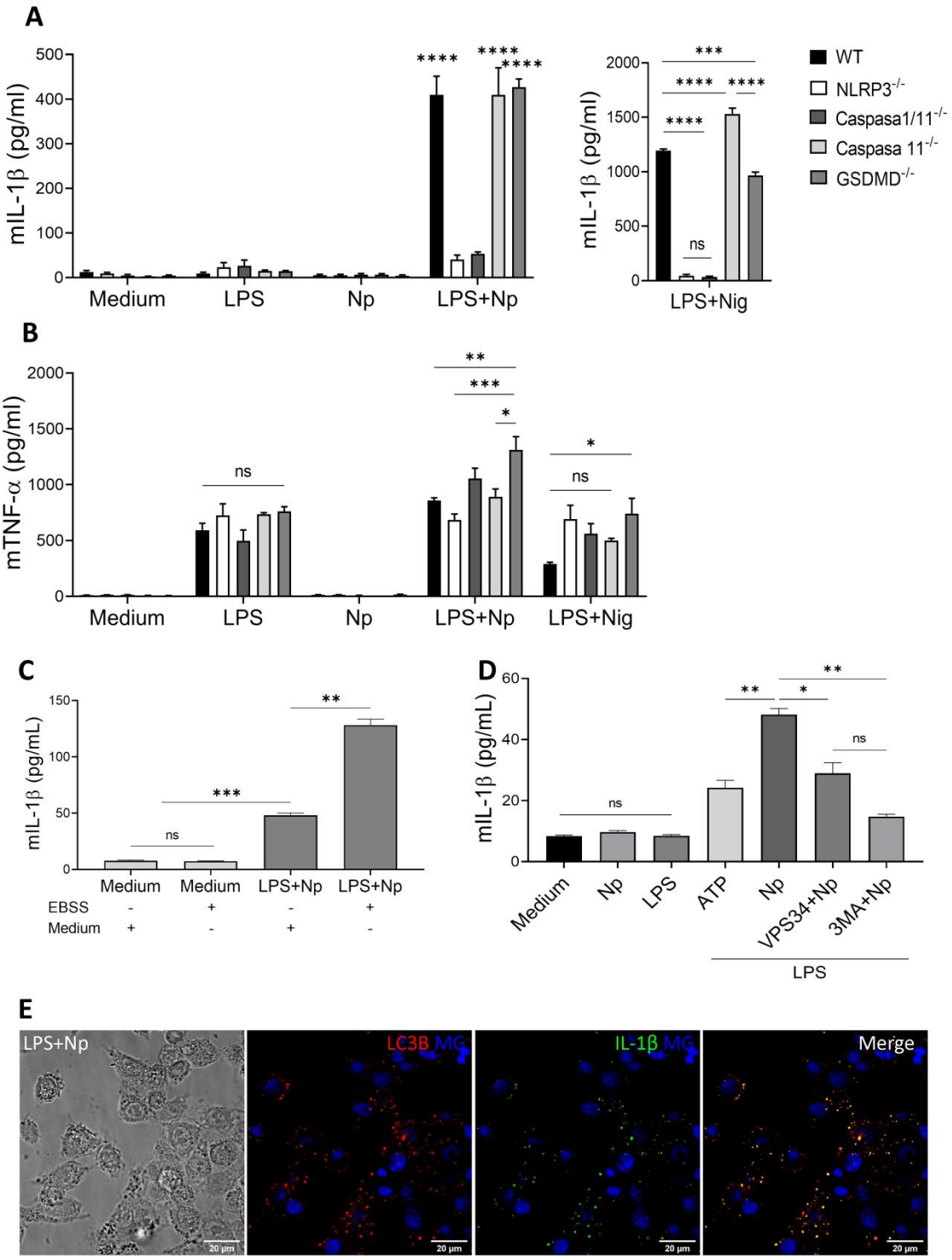

806

807 **Figure 4: Inflammasome pathway analysis in BMDM from C57BL/6 (WT), NLRP3$^{-/-}$,**

808 **Casp1/11$^{-/-}$, Casp11$^{-/-}$, GSDMD$^{-/-}$ mice.** Cells were stimulated with LPS, Np, or

LPS+Np, and **(A)** mIL-1β, **(B)** mTNFα were measured in supernatants by ELISA. The effect of autophagy stimulation by starvation on macrophage IL-1β secretion was investigated in J774 cell lines. After being primed for 3 hours with LPS, the cells were treated with Np. Six hours later, the cells were either left untreated in medium or had their supernatants replaced with Earle's Balanced Salt Solution (EBSS) for an additional hour of culture and quantification **(C)** mIL-1β in the supernatants by ELISA. J774 cells line were stimulated for 6h with Np in the presence of inhibitors of the autophagy VPS34-IN1 and 3-methiladenine (3-MA) and quantification **(D)** mIL-1β. **(E)** Cytokine mIL-1β colocalized with LC3B by confocal microscopy after 6 hours of stimulation with LPS+Np (MG: Methyl green). Data are expressed as mean±SEM. P-value was determined by ordinary one-way ANOVA *P<0,05; **P<0,01; ***P<0,001; ****p<0,0001.

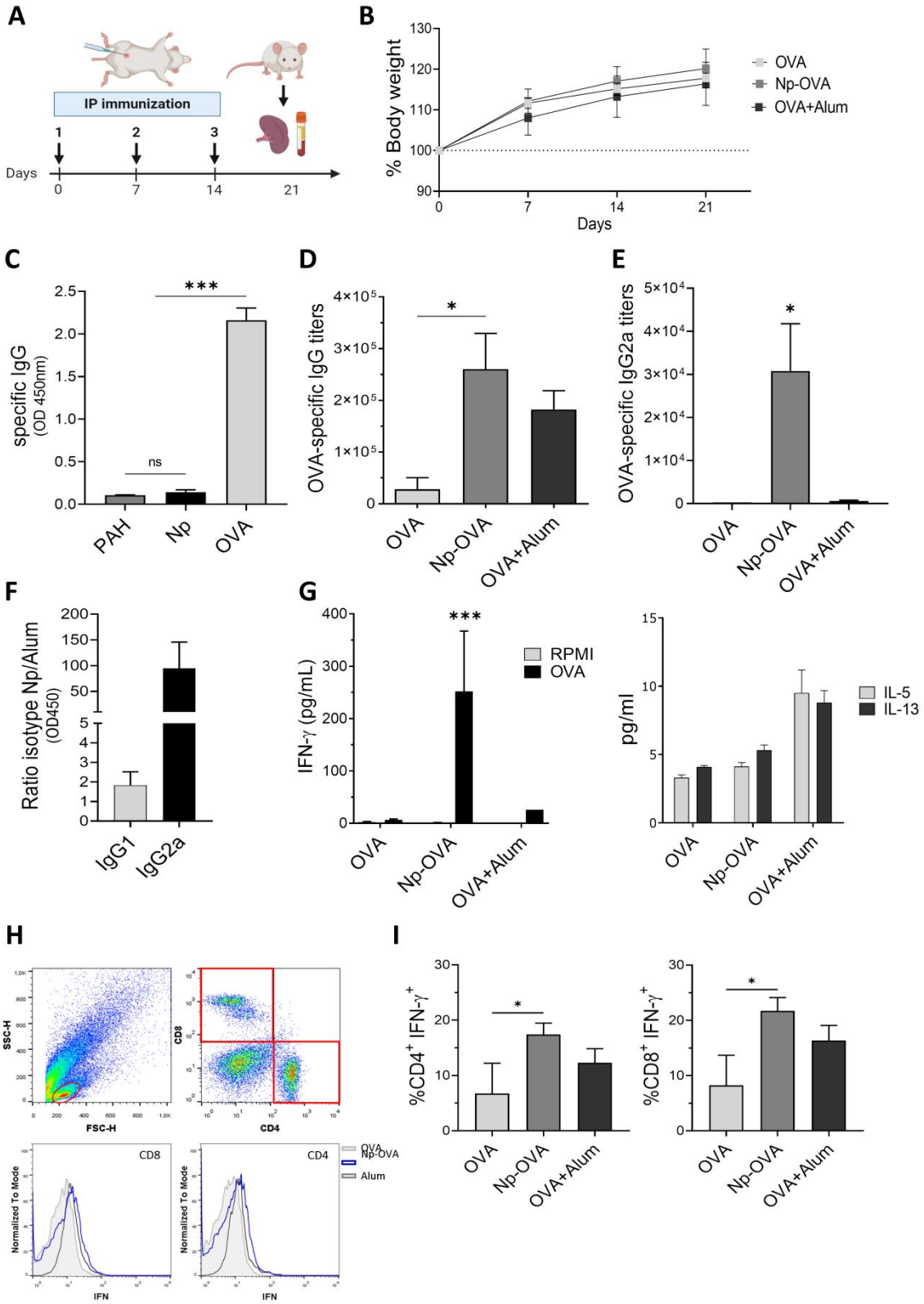
A
IP immunization
1
2
3
Days
0
7
14
21
B
% Body weight
Days
OVA
Np-OVA
OVA+Alum
C
specific IgG
(OD 450nm)
***
ns
PAH
Np
OVA
D
OVA-specific IgG titers
*
OVA
Np-OVA
OVA+Alum
E
OVA-specific IgG2a titers
*
OVA
Np-OVA
OVA+Alum
F
Ratio isotype Np/Alum
(OD450)
IgG1
IgG2a
G
IFN-γ (pg/mL)
***
RPMI
OVA
OVA
Np-OVA
OVA+Alum
pg/ml
IL-5
IL-13
OVA
Np-OVA
OVA+Alum
H
SSC-H
FSC-H
CD8
CD4
CD8
CD4
Normalized To Mode
IFN
OVA
Np-OVA
Alum
I
%CD4+ IFN-γ+
*
OVA
Np-OVA
OVA+Alum
%CD8+ IFN-γ+
*
OVA
Np-OVA
OVA+Alum

820

Figure 5: Intraperitoneally immunization of Balb/c mice with Np-OVA and specific humoral and cellular immune responses. (A) Immunization scheme; **(B)** Body weight monitoring; **(C)** quantification of serum specific IgG to PAH, Np and OVA and **(D)** OVA-Specific IgG and **(E)** IgG2a titers in serum of immunization animals and **(F)** serum optical density ratio of isotypes between Np-OVA and OVA+Alum; **(G)** Quantification of mIFN-γ, mIL-5 and mIL-13 in the supernatants of spleen cells from immunized mice assessed by ELISA. **(H)** Spleen cells from immunized mice were incubated with brefeldin A for the last 4h of culture and then were stained with anti-CD4 (PerCP-Cy5.5) or anti-CD8 (APC); flow cytometry gate strategy and Mean Fluorescent Intensity (MFI) **(I)** quantification for $CD4^{+}IFN\text{-}\gamma^{+}$ and $CD8^{+}IFN\text{-}\gamma^{+}$ T cells. The immunization experiment was carried out in duplicate and all experiments were performed in triplicate; data are expressed as mean±SEM. P-value was determined by ordinary one-way ANOVA *p<0,05; **p<0,01; ***p<0,001 or t-Student test #p<0,05.

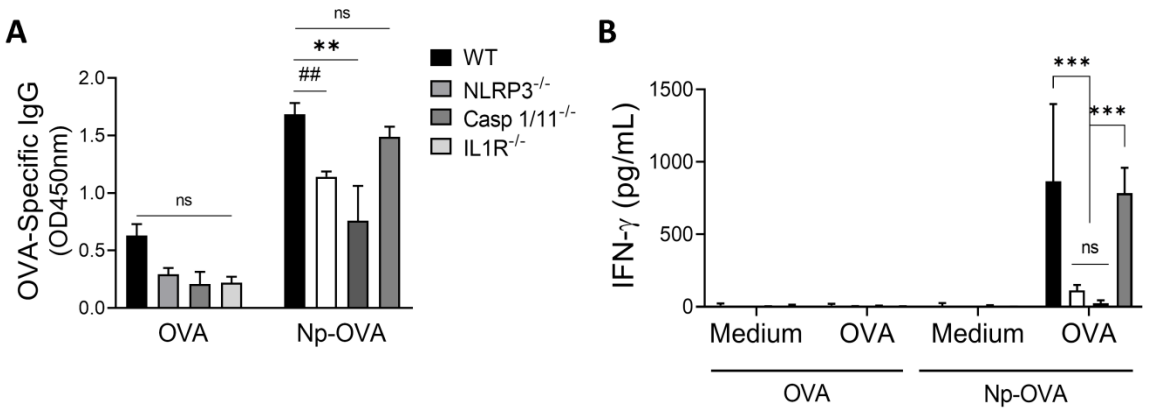

Figure 6: Intraperitoneal immunization with Np-OVA in WT and KO C57BL/6 mice and specific humoral and cellular response. C57BL/6 (WT), $NLRP3^{-/-}$, $Casp1/11^{-/-}$, $IL\text{-}1R^{-/-}$ mice were immunized following the same scheme as in Figure 5A. **(A)** Measurement

of serum OVA-specific IgG in serum (dilution 1/100) by ELISA and **(B)** secreted mIFN-γ by spleen cells from OVA or Np-OVA immunized mice by ELISA. The immunization experiment was carried out in duplicate and all experiments were performed in triplicate; data are expressed as mean±SEM. P-value was determined by ordinary one-way ANOVA *p<0,05; **p<0,01; ***p<0,001 or t-Student test ##p<0,01.

SUPPLEMENTARY FIGURES

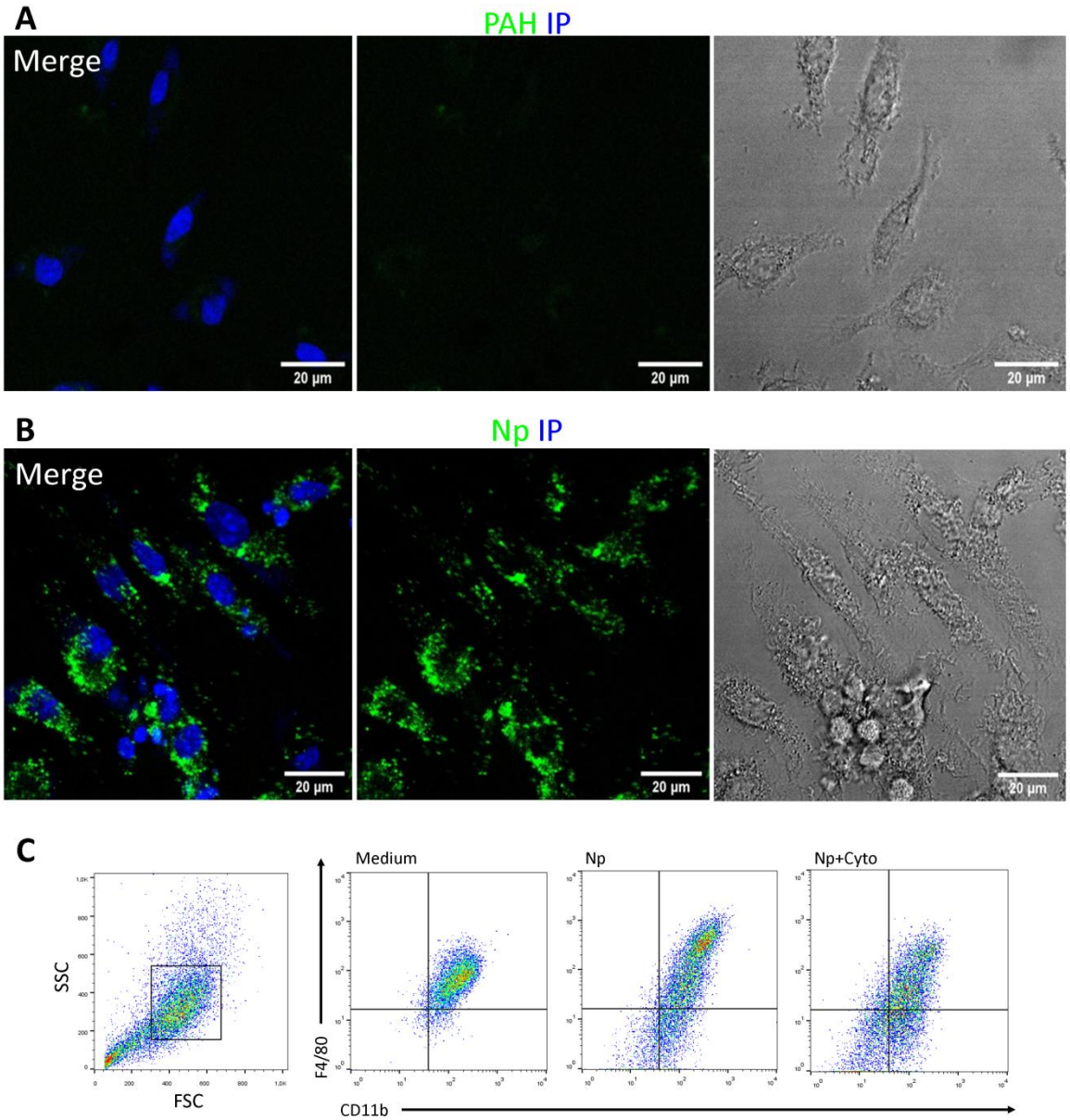

Figure S1: Internalization of (A) PAH-FITC (B) and Np-FITC in J774 macrophages by confocal microscopy. Representative images are shown. **(C)** Gate strategy to select F4/80 CD11b-positive macrophages cells.

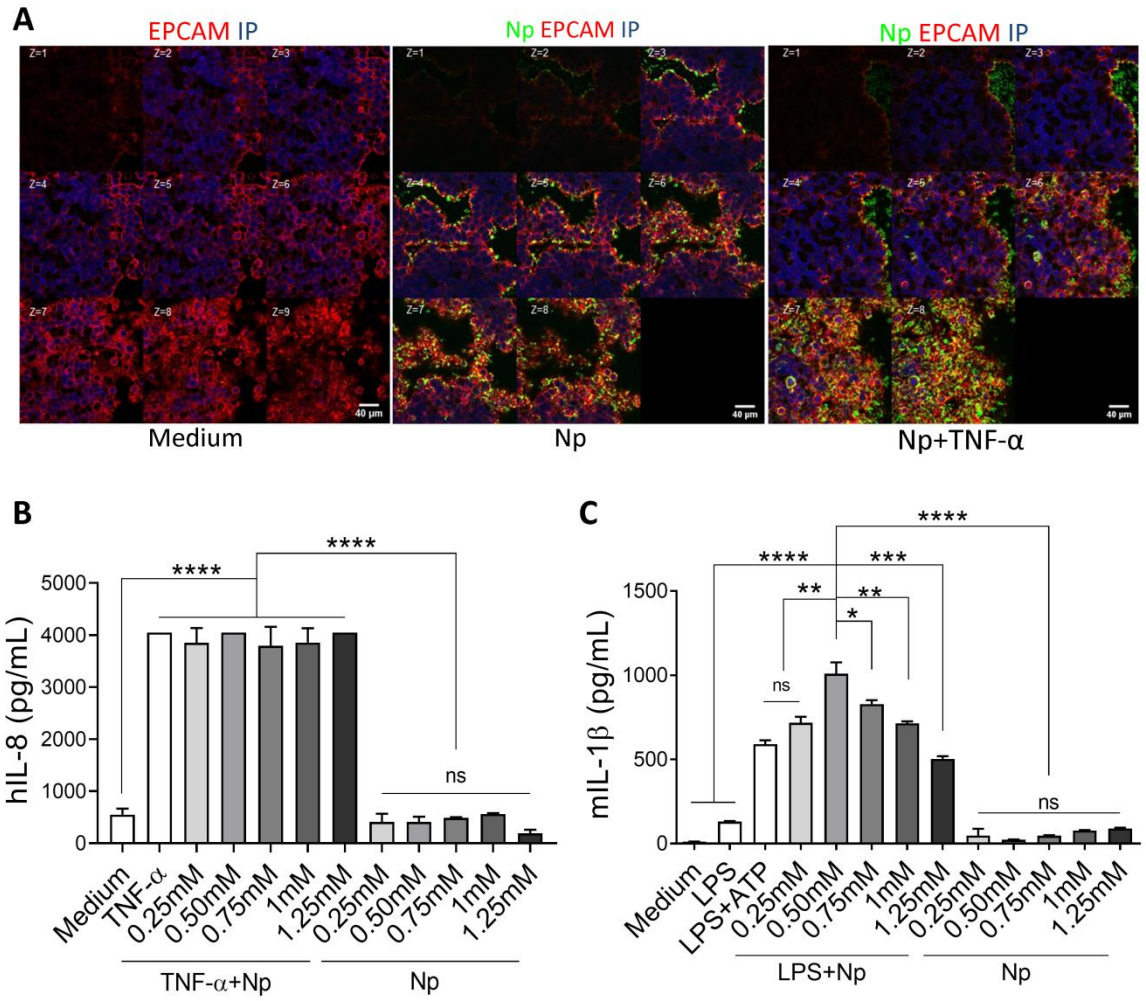

Figure S2: **Interaction of Np-FITC with human epithelial cell lines and dose-dependent cytokine response of cells to different stimuli. (A)** HT-29, different z-axis positions were scanned by confocal microscopy and EPCAM were used as a marker of epithelial cells. Representative images are shown. **(B)** Quantification of secreted hIL-8 in HT-29 cells exposed to medium, TNF-α, TNF-α+Np and Np; **(C)** Quantification of secreted mIL-1β in J774 macrophages exposed to medium, LPS, LPS+ATP, LPS+Np and Np. All experiments were carried out in triplicate and date are expressed as mean±SEM. P-value was determined by ordinary one-way ANOVA *p<0,05; **p<0,01; ***p<0,001; ****p<0,0001.

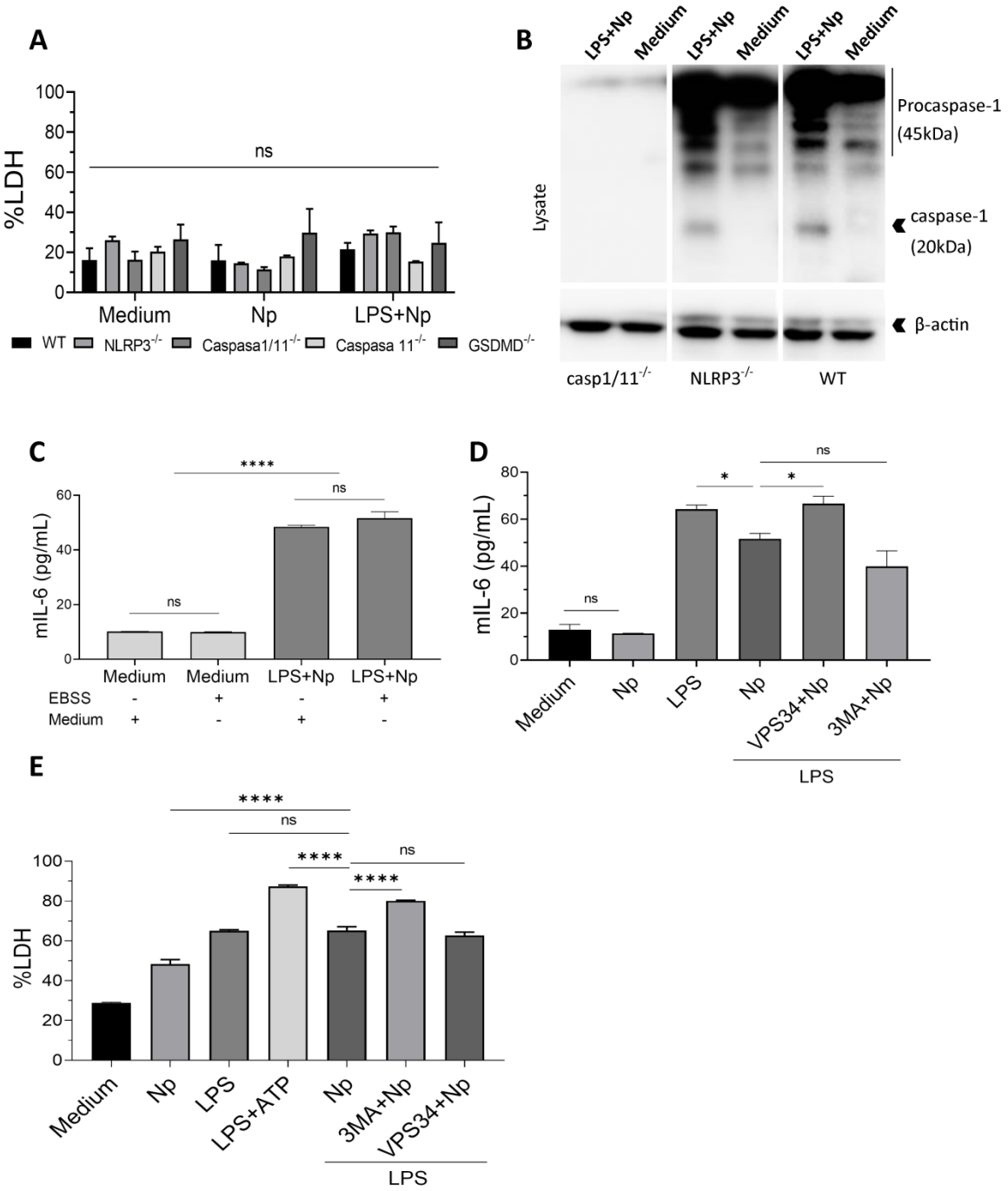
A
%LDH
ns
Medium
Np
LPS+Np
WT
NLRP3-/-
Caspasa1/11-/-
Caspasa 11-/-
GSDMD-/-
B
LPS+Np
Medium
Lysate
Procaspase-1
(45kDa)
caspase-1
(20kDa)
β-actin
casp1/11-/-
NLRP3-/-
WT
C
mIL-6 (pg/mL)
****
ns
EBSS
Medium
D
mIL-6 (pg/mL)
*
LPS
VPS34+Np
3MA+Np
E
%LDH
LPS+ATP

858

F

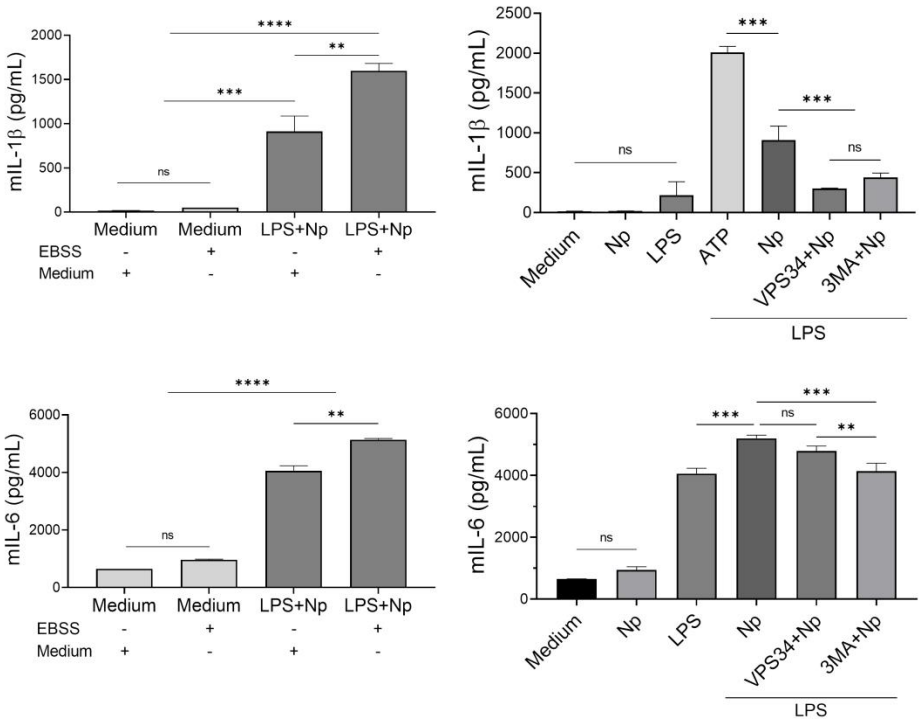
mIL-1β (pg/mL)
2000
1500
1000
500
0
****
**
***
ns
Medium
Medium
LPS+Np
LPS+Np
EBSS - + - +
Medium + - + -
2500
2000
1500
1000
500
0
***
***
ns
ns
Medium
Np
LPS
ATP
Np
VPS34+Np
3MA+Np
LPS
mIL-6 (pg/mL)
6000
4000
2000
0
****
**
ns
Medium
Medium
LPS+Np
LPS+Np
EBSS - + - +
Medium + - + -
6000
4000
2000
0
***
ns
***
**
ns
Medium
Np
LPS
Np
VPS34+Np
3MA+Np
LPS

G

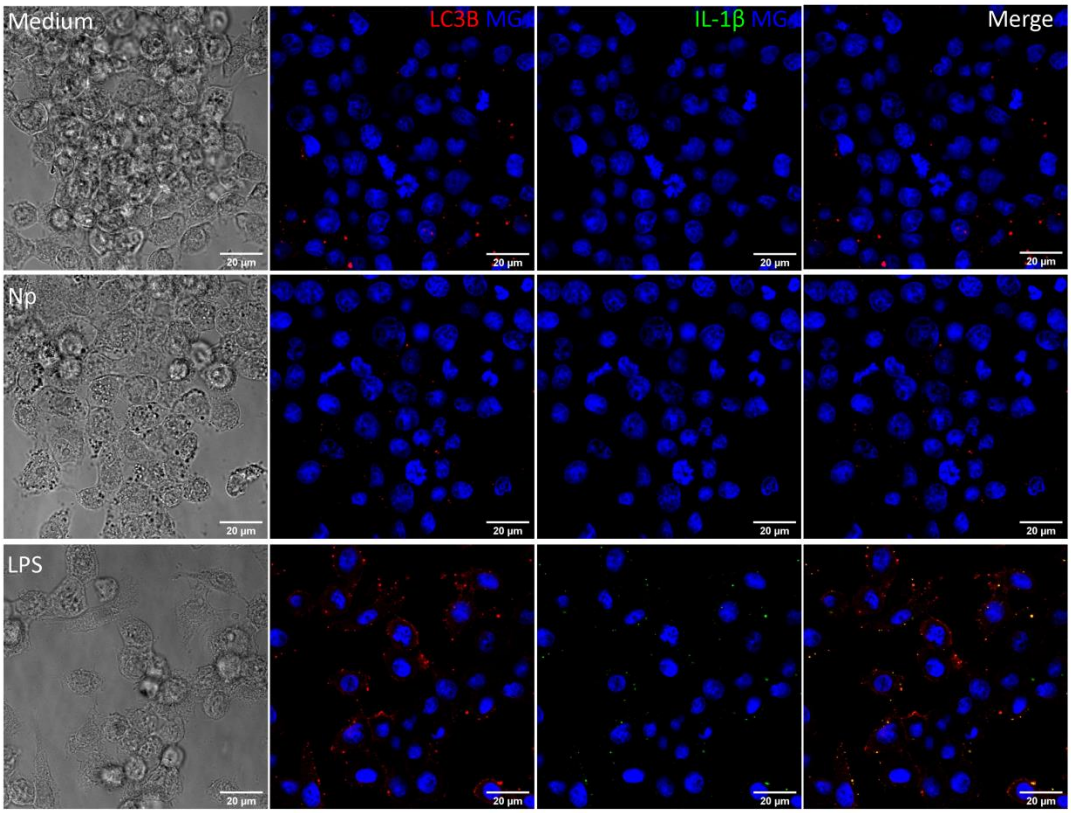
Medium
LC3B MG4
IL-1β MG4
Merge
Np
LPS
20 μm

859

Figure S3: **Inflammasome pathway analysis in BMDM from C57BL/6 (WT), NLRP3$^{-/-}$, Casp1/11$^{-/-}$, Casp11$^{-/-}$, GSDMD$^{-/-}$ mice.** Cells were stimulated with medium, Np or LPS+Np, and **(A)** %LDH were quantified in the supernatants and **(B)** caspase-1 activation was analyzed by immunoblotting in cell lysates using an antibody specific for the p20 subunit (20kDa) or the procaspase-1 (45kDa). J774 cell lines remained unstimulated or were stimulated with LPS. Three hours later, they were treated with Np. At 6 hours post-Np stimulation, cells were either left untreated (in medium) or their supernatants were removed and replaced with EBSS for an additional hour of culture. Subsequently J774 macrophages were stimulated for 6h with Np in the presence of inhibitors of the autophagy VPS34-IN1 and 3-methiladenine (3-MA) and quantification **(C-D)** mIL-6 and **(E)** %LDH in the supernatants. **(F)** Quantification of mIL-1β and mIL-6 in the supernatants of BMDCs after the treatment with autophagy inhibitors. **(G)** Medium, Np and LPS controls for the mIL-1β-LC3B colocalization by confocal microscopy. P-value was determined by ordinary one-way ANOVA *p<0,05; **p<0,01; ***p<0,001; ****p<0,0001.

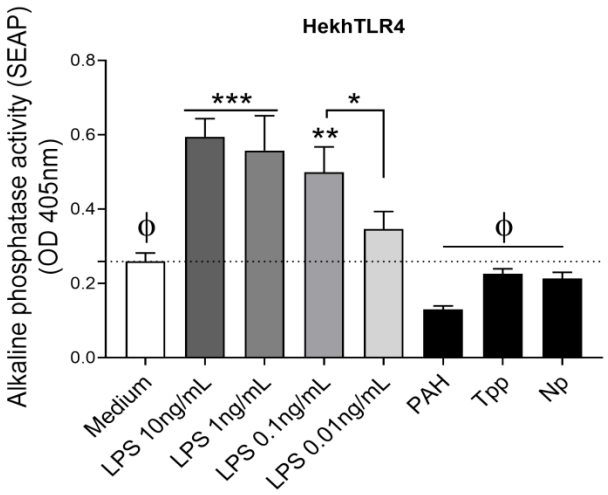

Figure S4: **Analysis of the stimulation of the Hek-hTLR4 cell line with LPS**. Different concentrations of LPS were included as positive controls; SEAP activity was measured in the supernatants. This experiment was performed in triplicate and data are expressed as mean±SEM. P-value was determined by ordinary one-way ANOVA *p<0,05; **p<0,01; ***p<0,001; Φ a result significantly different from LPS.

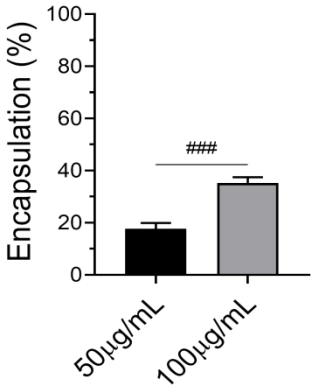

Figure S5: Analysis of the OVA encapsulation by Np. Free OVA was analyzed in the supernatant of the Np-OVA formulation by protein quantification (BCA). This experiment was performed in triplicate and data are expressed as mean±SEM. P-value was determined by Student's test ### p<0,001.